Obesity-induced overexpression of miRNA-143 inhibits insulin-stimulated AKT activation and impairs glucose metabolism

Sabine D. Jordan[1], Markus Krüger[2], Diana M. Willmes[1], Nora Redemann[1], F. Thomas Wunderlich[1], Hella S. Brönneke[3], Carsten Merkwirth[4], Hamid Kashkar[5], Vesa M. Olkkonen[6], Thomas Böttger[2], Thomas Braun[2], Jost Seibler[7] and Jens C. Brüning[1,8]

The contribution of altered post-transcriptional gene silencing to the development of insulin resistance and type 2 diabetes mellitus so far remains elusive. Here, we demonstrate that expression of microRNA (miR)-143 and 145 is upregulated in the liver of genetic and dietary mouse models of obesity. Induced transgenic overexpression of miR-143, but not miR-145, impairs insulin-stimulated AKT activation and glucose homeostasis. Conversely, mice deficient for the miR-143–145 cluster are protected from the development of obesity-associated insulin resistance. Quantitative-mass-spectrometry-based analysis of hepatic protein expression in miR-143-overexpressing mice revealed miR-143-dependent downregulation of oxysterol-binding-protein-related protein (ORP) 8. Reduced ORP8 expression in cultured liver cells impairs the ability of insulin to induce AKT activation, revealing an ORP8-dependent mechanism of AKT regulation. Our experiments provide direct evidence that dysregulated post-transcriptional gene silencing contributes to the development of obesity-induced insulin resistance, and characterize the miR-143–ORP8 pathway as a potential target for the treatment of obesity-associated diabetes.

Type 2 diabetes mellitus (T2DM) has reached epidemic proportions worldwide. The rapid increase in T2DM over the past decades has been caused by the interaction of genetic susceptibility and environmental factors such as inappropriate diet and sedentary lifestyle[1]. Resistance to the pleiotropic effects of insulin represents a key process in the development of the disease[2–5], but the underlying molecular mechanism(s) of insulin resistance are only partially understood and heterogeneous in nature. Among these, polymorphisms in genes that encode for proteins of the insulin signalling cascade and transcriptional dysregulation of these genes, and post-translational modifications and protein degradation contribute to the pathogenesis of T2DM (refs 6–11). The discovery of post-transcriptional gene silencing as an additional regulatory principle to control protein expression raises the possibility that microRNAs (miRNAs) are also involved in the development of obesity-induced insulin resistance and T2DM.

miRNAs represent a class of small, non-coding RNAs that are widely expressed in all multicellular organisms to regulate gene expression post-transcriptionally by cleavage or translational repression of their specific target mRNAs (refs 12–15). A role for miRNAs in metabolism was first described in *Drosophila melanogaster*, where loss of miR-14 increases body fat content[16]. In vertebrates, the first miRNA linked to metabolism was the pancreatic-islet-enriched miR-375, which interferes with insulin secretion[17]. Since then, regulatory functions have been described for miRNAs in all tissues directly targeted by insulin, such as brain, skeletal muscle, adipose tissue and liver[18]. Interestingly, whole-genome association studies for T2DM susceptibility genes revealed that most of the associated variants were located in non-coding regions[19,20], further supporting the possibility that regulatory, non-coding RNAs such as miRNAs may also contribute to the development of insulin resistance and T2DM.

[1]Department of Mouse Genetics and Metabolism, Institute for Genetics, Cologne Excellence Cluster on Cellular Stress Responses in Aging Associated Diseases (CECAD) and Center of Molecular Medicine Cologne (CMMC) University of Cologne, and Center for Endocrinology, Diabetes and Preventive Medicine (CEDP), University Hospital Cologne, Max Planck Institute for Neurological Research, Zülpicher Straße 47, D-50674 Cologne, Germany. [2]Max Planck Institute for Heart and Lung Research, D-61231 Bad Nauheim, Germany. [3]Phenotyping Facility of the Cologne Excellence Cluster on Cellular Stress Responses in Aging Associated Diseases (CECAD), D-50674 Cologne, Germany. [4]Institute for Genetics, Cologne Excellence Cluster on Cellular Stress Responses in Aging Associated Diseases (CECAD) and Center of Molecular Medicine Cologne (CMMC), University of Cologne, D-50674 Cologne, Germany. [5]Institute for Medical Microbiology, Immunology and Hygiene, Cologne Excellence Cluster on Cellular Stress Responses in Aging Associated Diseases (CECAD) and Center of Molecular Medicine Cologne (CMMC), University of Cologne, D-50674 Cologne, Germany. [6]Minerva Foundation Institute for Medical Research, Biomedicum, FI-00290 Helsinki, Finland. [7]TaconicArtemis Pharmaceuticals GmbH, D-51063 Cologne, Germany.
[8]Correspondence should be addressed to J.C.B. (e-mail: jens.bruening@uni-koeln.de)

As the liver plays a central role in glucose and lipid metabolism, and hepatic insulin resistance is a hallmark feature of T2DM, we analysed the hepatic miRNA expression pattern in genetically as well as diet-induced obese insulin-resistant mice and validated the functional role of altered miRNA expression on glucose metabolism *in vivo*.

RESULTS

Expression of miR-143 and miR-145 is upregulated in the liver of obese mouse models

To identify miRNAs undergoing metabolic regulation and potentially contributing to the development of obesity-associated disturbances in glucose and lipid metabolism, we first cloned small RNA molecules from the liver of mice, which either had free access to food (random fed), had been food restricted (fasted) or had been fasted and refed (refed). Sequencing of 312 concatamers in total, cloned from pooled hepatic total RNAs obtained under these conditions, revealed 1,070 small RNA sequences, of which 20.65% represented known miRNAs (see Supplementary Table S1a). Moreover, sequence analyses revealed the presence of 40 different miRNAs, with miR-122a as the predominant hepatic miRNA, representing 34.8% of the cloned miRNAs (see Supplementary Table S1b). Out of 32 miRNAs of which hepatic expression could be confirmed by northern-blot analysis, expression of miR-143 varied with feeding conditions (see Supplementary Table 1b and Fig. S1).

We next determined the expression of miR-143 in the liver of *db/db* mice, which are obese and diabetic owing to mutations of the leptin receptor gene[21,22]. This analysis revealed a significant 2.2-fold upregulation of miR-143 expression in the liver of *db/db* mice when compared with control mice (Fig. 1a). Similarly, expression of miR-143 was also significantly upregulated twofold in the liver of mice exposed to a high-fat diet when compared with control mice fed with a normal chow diet (Fig. 1b). Increased expression of miR-143 in the liver of both genetically and diet-induced obese mice was confirmed by quantitative real-time PCR analysis in independent cohorts of animals (Fig. 1c,d).

As miR-143 and miR-145, which form a small gene cluster on mouse chromosome 18, are co-expressed in several different tissues[23], we next investigated expression of miR-145 in the liver of obese mice. Quantitative real-time PCR analysis revealed significant upregulation of miR-145 expression in the liver of both *db/db* and diet-induced obese mice (Fig. 1e,f). Taken together, these experiments revealed upregulation of miR-143 and miR-145 expression in the liver of two different obesity mouse models.

To address whether altered expression of miR-143 and miR-145 is restricted to the liver of obese mice, we next determined their expression in various organs of *db/db* mice, compared with control mice. This analysis revealed significant upregulation of miR-143 in the heart and pancreas of *db/db* mice, whereas its expression was significantly reduced in white adipose tissue (Fig. 1g,h). Expression of miR-145 was significantly upregulated in skeletal muscle and pancreas of *db/db* mice (Fig. 1i,j). Thus, the miR-143–145 cluster is co-regulated in liver and pancreas of obese mice, whereas the regulation differs in other tissues.

Conditional overexpression of miR-143 in mice impairs glucose metabolism

To investigate whether increased hepatic miR-143 expression contributes to the metabolic phenotype arising from obesity *in vivo*,

we next aimed to mimic obesity-associated overexpression of this miRNA in a transgenic mouse model. As miRNAs have crucial roles in cellular differentiation and organ development[24], we aimed to circumvent potential developmental effects of upregulated miRNA expression and thus designed a strategy for time-controlled transgenic miRNA overexpression. We have previously demonstrated a tight regulation of transgenic short hairpin RNA (shRNa) expression from the *Rosa26* locus of mice under the control of a doxycycline-inducible H1 promoter[25,26]. Thus, we expanded this method to express miRNAs from the same locus. The doxycycline-inducible miRNA allele was generated by insertion of the respective miRNA coding sequence flanked by approximately 200 base pairs of the endogenous locus (Fig. 2a–c). Northern-blot analysis of miR-143 expression in control (wild-type) and miR-143 transgenic mice (miR-143[DOX]) after four weeks of doxycycline treatment revealed significant overexpression of miR-143 in liver and brown adipose tissue of miR-143[DOX] mice, whereas expression from the H1 promoter failed to raise miR-143 concentration above the relatively high endogenous levels in skeletal muscle and white adipose tissue (Fig. 2d,e). Importantly, in isolated hepatocytes northern-blot analysis revealed both endogenous miR-143 expression in control and doxycycline-induced overexpression in transgenic hepatocytes (Fig. 2f). Comparative time-course analysis of miR-143 expression in liver and skeletal muscle revealed tight doxycycline-dependent miR-143 overexpression, as in the absence of doxycycline, basal miR-143 expression was comparable between miR-143[DOX] and control mice. However, doxycycline administration led to rapid induction of miR-143 overexpression in the liver of miR-143[DOX] mice after only one day of treatment (Fig. 2g). Thus, our approach provides a versatile tool to conditionally overexpress miRNAs in mice.

As we had identified upregulated miR-143 expression in the liver of obese mice, we first investigated whether conditional overexpression of miR-143, predominantly in liver and brown adipose tissue, affects energy homeostasis. Nevertheless, this analysis revealed unaltered body weight, fat mass and circulating plasma leptin concentrations, as an indirect measure of adiposity, in miR-143[DOX] mice, compared with control mice (see Supplementary Fig. S2a–c). Moreover, food intake, body temperature and energy expenditure remained unaltered in miR-143[DOX] mice, compared with control mice (see Supplementary Fig. S2d–f). Analysis of brown-adipose-tissue morphology and expression of key regulators of brown-adipose-tissue differentiation and function revealed no significant differences between miR-143[DOX] and control mice (see Supplementary Fig. S2g,h). Thus, conditional overexpression of miR-143 as present in obese mice does not alter energy homeostasis or specifically affect brown-adipose-tissue function.

However, doxycycline-induced overexpression of miR-143 resulted in a prominent dysregulation of glucose metabolism. Although fasting blood glucose concentrations did not differ between miR-143[DOX] and control littermates in either the absence or presence of doxycycline, doxycycline-treated miR-143[DOX] mice exhibited significantly increased fasting plasma insulin concentrations (Fig. 3a,b). Moreover, although glucose-tolerance tests did not differ between miR-143[DOX] and control mice in the absence of doxycycline, we detected a significantly impaired glucose tolerance in miR-143[DOX] mice after induction of miR-143 overexpression (Fig. 3c). Similarly, insulin sensitivity did not differ
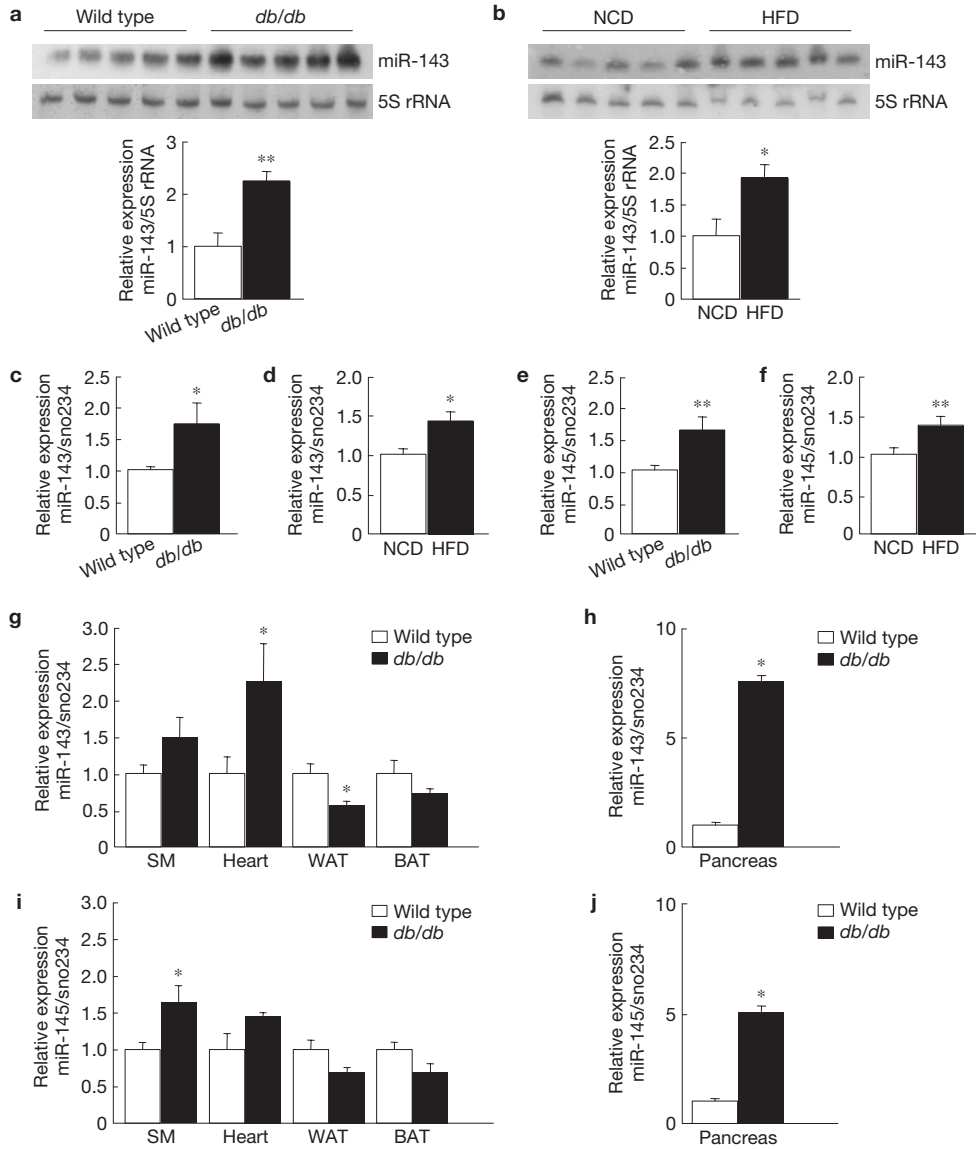
Figure 1 Dysregulated expression of the miR-143–145 cluster in insulin target tissues of obese and diabetic mice. (**a**) Northern-blot analysis of hepatic miR-143 expression in *db/db* mice ($n = 5$), compared with wild-type controls ($n = 5$). 5S ribosomal RNA was used as a loading control. (**b**) Northern-blot analysis of hepatic miR-143 expression in mice fed high-fat diet (HFD; $n = 5$) or normal chow diet (NCD) ($n = 5$). 5S rRNA was used as a loading control. (**c**) Real-time PCR analysis of hepatic miR-143 expression in *db/db* mice ($n = 10$), compared with wild-type controls ($n = 10$). (**d**) Real-time PCR analysis of hepatic miR-143 expression in mice fed high-fat diet (HFD; $n = 8$) or normal chow diet (NCD; $n = 5$). (**e**) Real-time PCR analysis of hepatic miR-145 expression in *db/db* mice ($n = 10$), compared with wild-type controls ($n = 10$). (**f**) Real-time PCR analysis of hepatic miR-145 expression in mice fed high-fat diet (HFD; $n = 8$) or normal chow diet (NCD; $n = 5$). (**g**) Real-time PCR analysis of miR-143

expression in the indicated tissues of *db/db* mice (skeletal muscle (SM), $n = 8$; heart, $n = 7$; white adipose tissue (WAT), $n = 7$; brown adipose tissue (BAT), $n = 8$), compared with wild-type controls (SM, $n = 7$; heart, $n = 9$; WAT, $n = 9$; BAT, $n = 9$). (**h**) Real-time PCR analysis of pancreatic miR-143 expression in *db/db* mice ($n = 6$), compared with wild-type controls ($n = 5$). (**i**) Real-time PCR analysis of miR-145 expression in the indicated tissues of *db/db* mice (SM, $n = 7$; heart, $n = 6$; WAT, $n = 7$; BAT, $n = 8$), compared with wild-type controls (SM, $n = 8$; heart, $n = 7$; WAT, $n = 8$; BAT, $n = 6$). (**j**) Real-time PCR analysis of pancreatic miR-145 expression in *db/db* mice ($n = 6$, 20 weeks old), compared with wild-type controls ($n = 5$, 20 weeks old). Expression of miRNAs was normalized to that of control RNAs (northern blot, 5S rRNA; real-time PCR, sno234) and set to unity in wild-type controls. All error bars indicate s.e.m. $^*P \leq 0.05$, $^{**}P \leq 0.01$. Uncropped images of blots are shown in Supplementary Fig. S9.

between miR-143^DOX and control mice in the absence of doxycycline, but doxycycline-treated miR-143^DOX mice exhibited significantly impaired insulin tolerance (Fig. 3d). Consistently, homeostatic model assessment (HOMA) indices of doxycycline-treated miR-143^DOX mice were significantly increased, further indicating reduced insulin sensitivity of these mice (Fig. 3e).

Analysis of glucose-stimulated insulin secretion, morphological analysis of pancreatic β-cell islets and determination of pancreatic β-cell mass revealed no alterations (Fig. 3f–h), further supporting the hypothesis that impaired glucose metabolism in miR-143^DOX mice arises primarily from insulin resistance rather than impaired insulin secretion due to β-cell dysfunction.
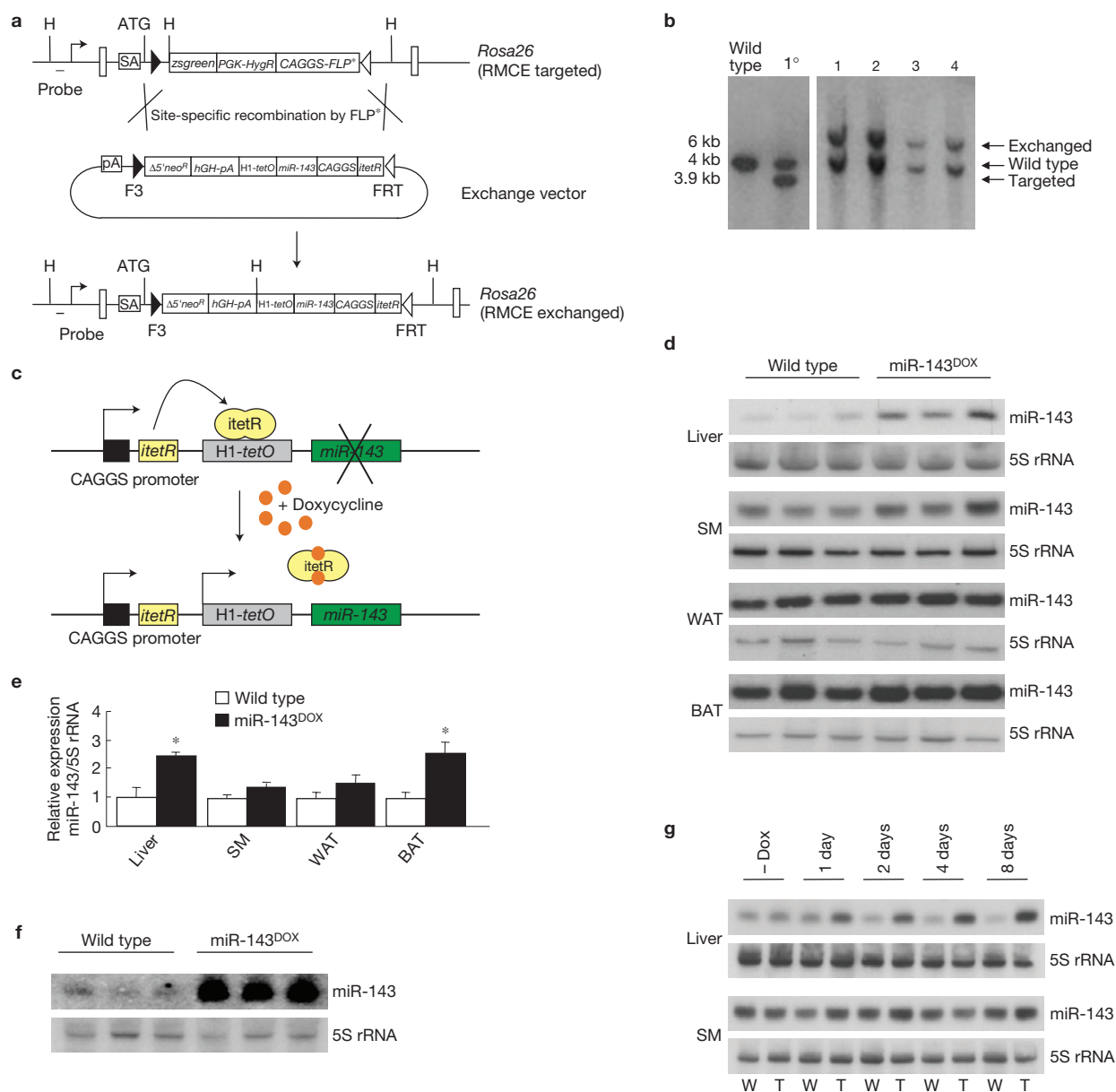
Figure 2 Conditional overexpression of miR-143 in mice. (**a**) Scheme of a single vector configuration for inducible miRNA expression. Recombinase-mediated cassette exchange (RMCE) through Flp[e]-mediated recombination using the exchange vector generates the *Rosa26* (RMCE-exchanged) allele. The exchange vector carries the miR-143 coding region under the control of the H1-*tetO* promoter, the codon-optimized *itetR* gene under the control of the CAGGS promoter (chicken β-actin promoter) and a truncated *neo[R]* gene for positive selection of clones on successful RMCE. (**b**) Southern-blot analysis of genomic DNA from embryonic stem cells. In clones 1–4 successful RMCE had occurred. The positions of probe and restriction sites (H = HindIII) are indicated in **a**. Clone 2 was used for generation of transgenic mice. (**c**) Schematic representation of transgene for inducible miR-143 overexpression. Expression of transgenic miR-143 relies on the RNA polymerase III (polIII)-dependent H1 promoter, containing the operator sequences (*tetO*) of the *Escherichia coli* tetracycline-resistance operon. Binding of the tetracycline-resistance-operon repressor (itetR) to

tetO prevents transcription. Doxycycline sequesters itetR and enables the binding of polIII to the H1 promoter, resulting in transcription of the extra *miR-143* allele. (**d**) Northern-blot analysis of mature miR-143 and 5S rRNA (loading control) in liver, skeletal muscle (SM) and white (WAT) and brown adipose tissue (BAT) of miR-143[DOX] mice and wild-type littermate controls. (**e**) Quantification of northern-blot analysis shown in **d** (miR-143[DOX] mice, *n* = 3; wild-type littermate controls, *n* = 3). Expression of miR-143 in the indicated tissues was normalized to that of 5S rRNA and set to unity in the respective wild-type tissue. All error bars indicate s.e.m. *$P \leq 0.05$. (**f**) Northern-blot analysis of mature miR-143 and 5S rRNA (loading control) in hepatocytes isolated from miR-143[DOX] mice and wild-type littermate controls. (**g**) Northern-blot analysis of mature miR-143 and 5S rRNA (loading control) in liver and skeletal muscle (SM) of miR-143[DOX] mice (T) and wild-type littermate controls (W) without and after 1, 2, 4 and 8 days of doxycycline administration. Uncropped images of blots are shown in Supplementary Fig. S9.

To investigate whether the observed alterations in glucose metabolism are the specific result of transgenic overexpression of miR-143, we carried out the same analyses of energy homeostasis

and glucose metabolism in a second line of transgenic mice, where an shRNA directed to the β-galactosidase gene (*LacZ* shRNA) was expressed using the same strategy (Fig. 4a). We did not
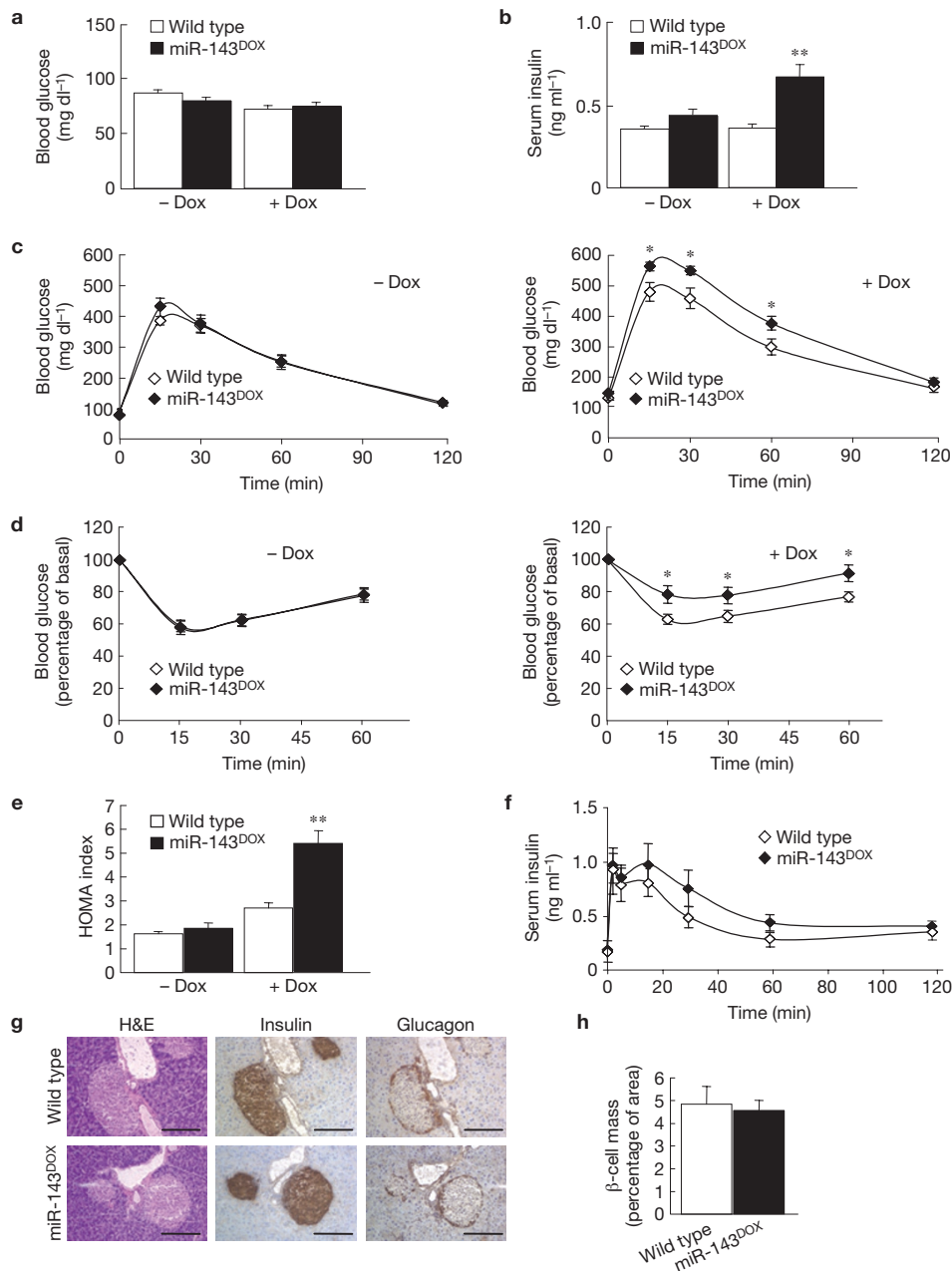
Figure 3 Impaired glucose metabolism in miR-143-overexpressing mice. (**a**) Blood glucose concentrations of miR-143^{DOX} mice (−Doxycycline (Dox), $n = 22$; +Dox, $n = 11$) and wild-type littermate controls (−Dox, $n = 22$, +Dox, $n = 10$) before and after doxycycline administration. Concentrations were measured in overnight-fasted mice. (**b**) Serum insulin levels of miR-143^{DOX} mice (−Dox, $n = 7$; +Dox, $n = 13$) and wild-type littermate controls (−Dox, $n = 9$; +Dox, $n = 13$) before and after doxycycline administration. Concentrations were measured in overnight-fasted mice. (**c**) Glucose-tolerance test of miR-143^{DOX} mice (−Dox, $n = 15$; +Dox, $n = 13$) and wild-type littermate controls (−Dox, $n = 16$; +Dox, $n = 13$) before and after doxycycline administration. (**d**) Insulin-tolerance test of miR-143^{DOX} mice (−Dox, $n = 14$; +Dox, $n = 22$) and wild-type littermate controls (−Dox, $n = 15$; +Dox, $n = 19$) before and after doxycycline administration. Blood glucose concentrations of miR-143^{DOX} mice and wild-type controls before i.p. administration of insulin were set to 100%. (**e**) HOMA of miR-143^{DOX} mice (−Dox, $n = 16$; +Dox, $n = 13$) and wild-type littermate controls (−Dox, $n = 16$; +Dox, $n = 13$) before and after doxycycline administration. (**f**) Plasma insulin concentrations after glucose bolus injection in miR-143^{DOX} mice ($n = 8$) and wild-type littermate controls ($n = 9$). (**g**) Haematoxylin and eosin (H&E), insulin and glucagon stainings of pancreatic islets in miR-143^{DOX} mice and wild-type littermate controls. Scale bars 100 μm. (**h**) Percentage of β-cell mass in miR-143^{DOX} mice ($n = 5$) and wild-type littermate controls ($n = 5$). All error bars indicate s.e.m. $^*P \leq 0.05$, $^{**}P \leq 0.01$.

find any evidence that induced expression of *LacZ* shRNA altered body weight (Fig. 4b) or changed glucose tolerance or insulin sensitivity in these mice (Fig. 4c–f). Moreover, mice with conditional overexpression of miRNA-145 did not exhibit any alterations in energy or glucose homeostasis (Fig. 4g–l). Collectively, these experiments revealed that inducible overexpression of miR-143 specifically impairs glucose metabolism through induction of insulin resistance.
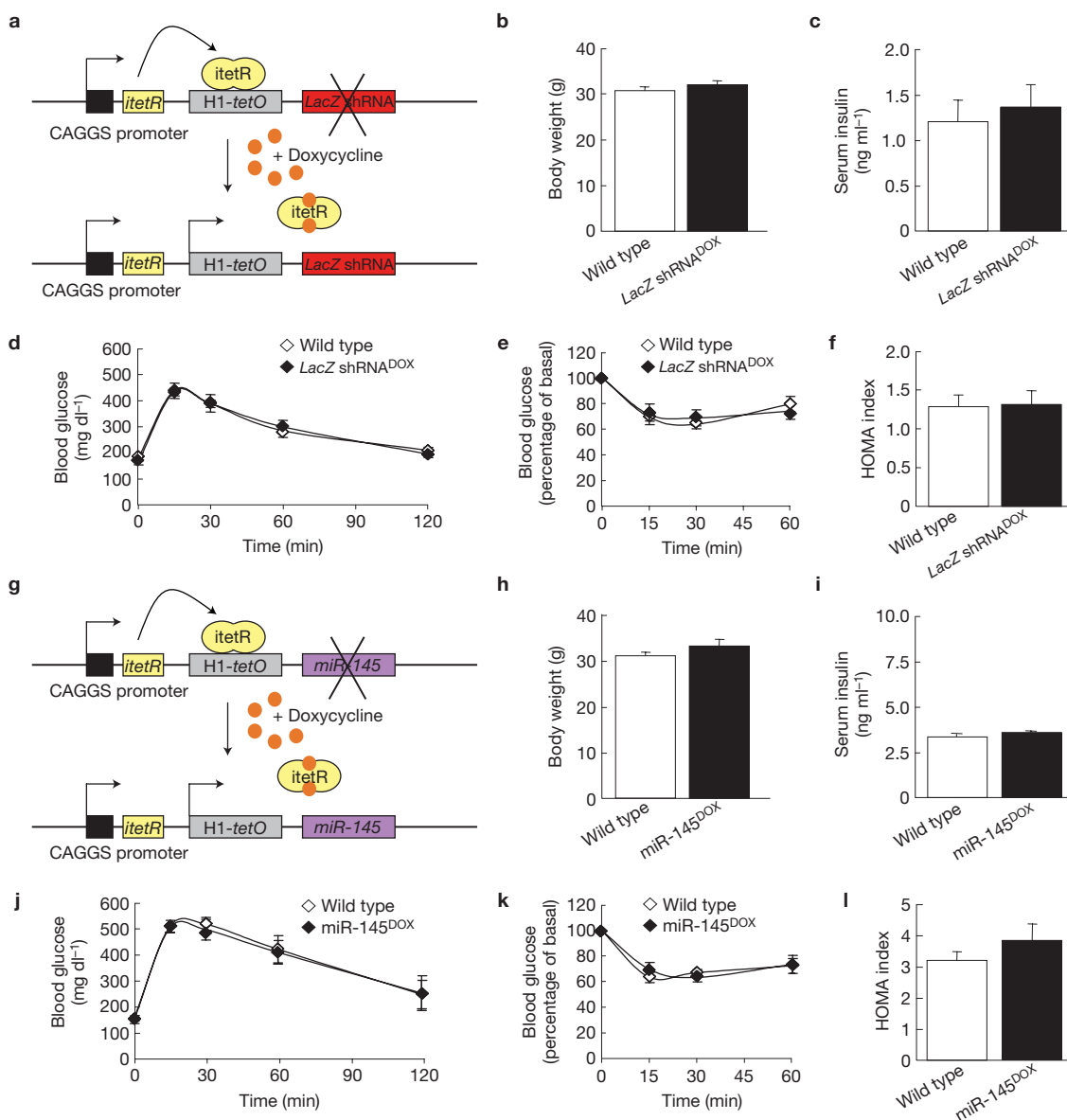
Figure 4 Conditional overexpression of *LacZ* shRNA or miR-145 does not impair glucose homeostasis. (**a**) Schematic representation of transgene for inducible *LacZ* shRNA expression. (**b**) Body weight of *LacZ* shRNA^{DOX} mice ($n = 10$) and wild-type littermate controls ($n = 10$). (**c**) Serum insulin levels of *LacZ* shRNA^{DOX} mice ($n = 10$) and wild-type littermate controls ($n = 10$). Concentrations were measured in overnight-fasted mice. (**d**) Glucose-tolerance test of *LacZ* shRNA^{DOX} mice ($n = 10$) and wild-type littermate controls ($n = 10$). (**e**) Insulin-tolerance test of *LacZ* shRNA^{DOX} mice ($n = 10$) and wild-type littermate controls ($n = 10$). Blood glucose concentrations of *LacZ* shRNA^{DOX} mice and wild-type controls before i.p. administration of insulin were set to 100%. (**f**) HOMA of *LacZ* shRNA^{DOX} mice ($n = 10$) and wild-type littermate controls ($n = 10$). (**g**) Schematic representation of transgene for inducible miR-145 overexpression. (**h**) Body weight of miR-145^{DOX} mice ($n = 6$) and wild-type littermate controls ($n = 7$). (**i**) Serum insulin levels of miR-145^{DOX} mice ($n = 8$) and wild-type littermate controls ($n = 8$). Concentrations were measured in overnight-fasted mice. (**j**) Glucose-tolerance test of miR-145^{DOX} mice ($n = 6$) and wild-type littermate controls ($n = 7$). (**k**) Insulin-tolerance test of miR-145^{DOX} mice ($n = 6$) and wild-type littermate controls ($n = 7$). Blood glucose concentrations of miR-145^{DOX} mice and wild-type controls before i.p. administration of insulin were set to 100%. (**l**) Homeostatic model assessment of miR-145^{DOX} mice ($n = 8$) and wild-type littermate controls ($n = 8$). All error bars indicate s.e.m.

Impaired insulin-stimulated AKT activation in the liver of miR-143 transgenic mice

To further investigate the molecular basis of insulin resistance in miR-143^{DOX} mice, we analysed insulin-stimulated signalling in liver and skeletal muscle. Following intravenous (i.v.) insulin injection, tyrosine phosphorylation of the insulin receptor was unaltered in these organs of miR-143^{DOX} when compared with control mice (Fig. 5a,b). Furthermore, hepatic expression and insulin-stimulated tyrosine phosphorylation of insulin receptor

substrate 1 (IRS-1) was comparable between miR-143^{DOX} and control mice.

In contrast, phosphorylation and thus activation of the downstream serine/threonine kinase AKT was significantly reduced in liver, but not skeletal muscle, of miR-143^{DOX} mice (Fig. 5a,b), consistent with increased miR-143 expression in liver, but not skeletal muscle. Taken together, these experiments indicate that miR-143 selectively inhibits insulin signalling at the level of AKT activation, whereas upstream receptor signalling remains intact.
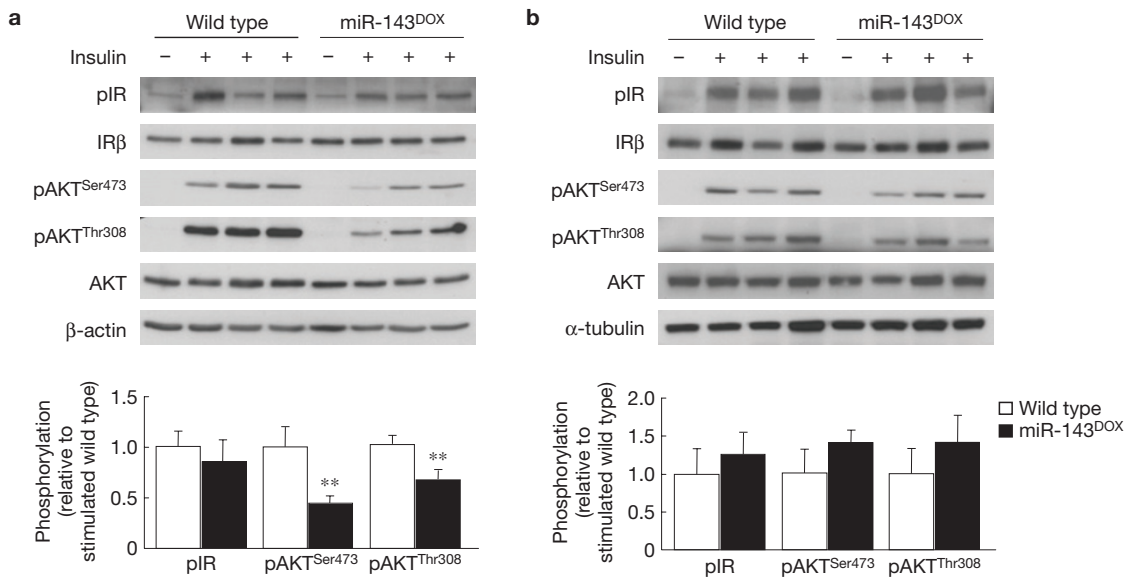
Figure 5 Conditional miR-143 overexpression impairs insulin-stimulated AKT activation in liver. (**a**) Representative western-blot analysis and quantification of expression and insulin-stimulated phosphorylation of IR and AKT in the liver of miR-143[DOX] mice (pIR, $n = 15$; pAKT[Ser473], $n = 14$; pAKT[Thr308], $n = 15$) and wild-type littermate controls (pIR, $n = 16$; pAKT[Ser473], $n = 17$, pAKT[Thr308], $n = 17$). β-actin was used as a loading control. (**b**) Representative western-blot analysis and quantification of expression and insulin-stimulated phosphorylation of IR and AKT in skeletal muscle of miR-143[DOX] mice ($n = 5$) and wild-type littermate controls ($n = 5$). α-tubulin was used as a loading control. Mice were injected with either saline (−) or insulin (+). Immunoreactive phospho-proteins were normalized to the total expression of the respective protein and the quotient of wild-type controls was set to unity. All error bars indicate s.e.m. **$P \leq 0.01$. Uncropped images of blots are shown in Supplementary Fig. S9.

To further determine the functional consequence of inducible miR-143 overexpression, we analysed hepatic gene expression in miR-143[DOX] mice. These experiments revealed a total of 205 genes that were significantly downregulated in livers of miR-143[DOX] mice when compared with controls, whereas 139 genes exhibited a significant, more than twofold, upregulation (see Supplementary Table S2). Disease-based gene-ontology analysis of dysregulated hepatic mRNAs revealed a significant enrichment of transcripts associated with endocrine-metabolic disorders, in particular T2DM. Network analysis of genes with altered expression in the liver of miR-143[DOX] mice implied in glucose and lipid metabolism revealed insulin-dependent phosphatidylinositol-3-OH kinase (PI(3)K) signalling as the predicted regulatory integrator of these two altered clusters (see Supplementary Fig. S3). These findings are in line with a pivotal role for AKT-dependent signalling in control of liver lipid and glucose metabolism[27] and further support a prominent role for miR-143 in the regulation of hepatic metabolic processes. Moreover, they are consistent with altered PI(3)K–AKT-dependent signalling causing the observed changes in glucose homeostasis and altered hepatic gene expression in miR-143[DOX] mice.

Mice deficient for miR-143–145 are protected from diet-induced insulin resistance and AKT inhibition

As overexpression of miR-143 as observed in obesity clearly induced insulin resistance and inhibition of insulin-stimulated AKT activation, we investigated whether miR-143 deficiency can protect against obesity-induced insulin resistance *in vivo*. To this end, we exposed miR-143–145-deficient[23] and control mice to high-fat feeding and compared glucose metabolism as well as hepatic insulin signalling in these mice. Glucose-tolerance tests revealed improved glucose

tolerance in obese miR-143–145-deficient mice (Fig. 6a). Moreover, the insulin sensitivity of obese miR-143–145-deficient mice was significantly improved when compared with controls (Fig. 6b). At a molecular level, improved insulin sensitivity was paralleled by increased insulin-stimulated phosphorylation of AKT in the liver of obese miR-143–145-deficient mice, compared with controls (Fig. 6c). Consistent with the results for conditional miR-143 overexpression under normal chow diet, miR-143–145 deficiency in the context of high-fat feeding did not affect body weight or circulating plasma leptin concentrations (see Supplementary Fig. S4a,b).

As miR-143 has previously been reported to regulate adipocyte differentiation *in vitro*[28], we further investigated the morphology of white adipose tissue in miR-143–145-deficient mice. However, consistent with unaffected body weight and fat mass, histological examination revealed unaltered tissue morphology and adipocyte size distribution in miR-143–145-deficient mice (Fig. 6d). Moreover, mRNA expression of markers for white adipose tissue differentiation and of genes implicated in lipid metabolism was comparable between miR-143–145-deficient and control mice (see Supplementary Fig. S4c–e). Taken together, these data indicate that altered adipogenesis does not underlie the observed protection against diet-induced insulin resistance.

As diet-induced insulin resistance has been demonstrated to arise from increased obesity-associated infiltration of white adipose tissue by macrophages and subsequent elevation of pro-inflammatory cytokines both locally and systemically, we investigated these parameters in obese miR-143–145-deficient and control mice. Immunohistochemical analysis of infiltrating, activated macrophages, however, demonstrated comparable numbers of Mac-2-positive cells in white adipose tissue (Fig. 6e). Consistently, mRNA expression of the macrophage marker F4/80 as well as the pro-inflammatory cytokines *interleukin 6* (*Il-6*) and
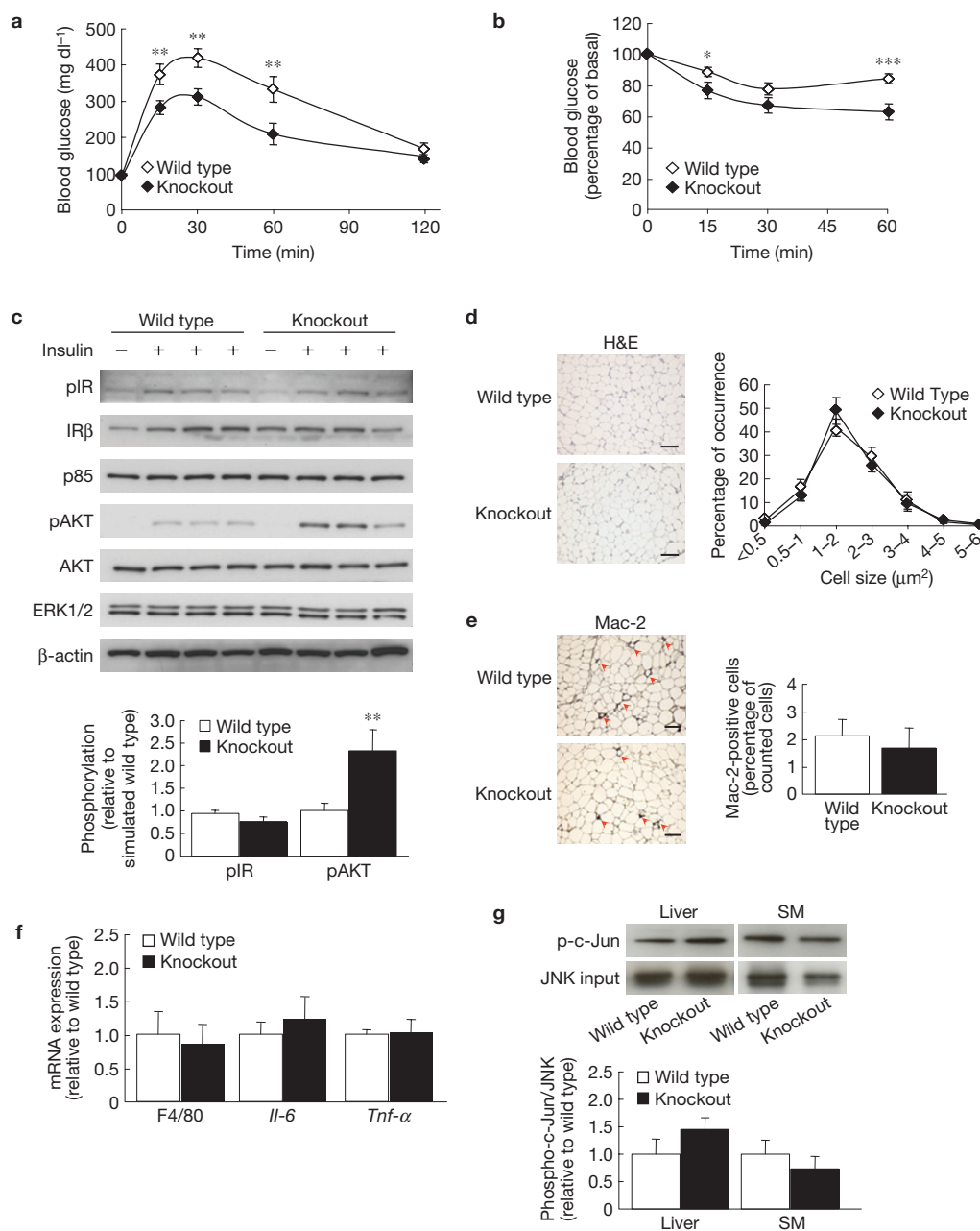
Figure 6 miR-143–145-deficient mice are protected from diet-induced insulin resistance and hepatic AKT inhibition. (**a**) Glucose-tolerance test of miR-143–145 knockout mice ($n = 12$) and wild-type littermate controls ($n = 12$), on a high-fat diet. (**b**) Insulin-tolerance test of miR-143–145 knockout mice ($n = 12$) and wild-type littermate controls ($n = 12$) on a high-fat diet. Blood glucose concentrations of miR-143–145 knockout mice and wild-type controls before i.p. administration of insulin were set to 100%. (**c**) Representative western-blot analysis and quantification of expression and insulin-stimulated phosphorylation of indicated proteins in the liver of miR-143–145 knockout mice (pIR, $n = 7$; pAKT, $n = 7$) and wild-type controls (pIR, $n = 8$; pAKT, $n = 8$) on a high-fat diet. Mice were injected with either saline ($-$) or insulin ($+$). Immunoreactive phospho-proteins were normalized to the total expression of the respective protein and the quotient of wild-type controls was set to unity. β-actin was used as a loading control. (**d**) Haematoxylin and eosin (H&E) staining and adipocyte size distribution of epigonadal white-adipose-tissue sections from

miR-143–145 knockout mice ($n = 3$) and wild-type controls ($n = 3$) on a high-fat diet. Scale bar 100 μm. (**e**) Mac-2 staining and quantification of white adipose tissue sections from miR-143–145 knockout mice ($n = 3$) and wild-type controls ($n = 3$) on a high-fat diet. Scale bar 100 μm. Red arrows indicate cells surrounded by a Mac-2-positive area. (**f**) Real-time PCR analysis of F4/80, Il-6 and Tnf-α mRNA expression in white adipose tissue of miR-143–145 knockout mice ($n = 5$), compared with wild-type controls ($n = 5$), on a high-fat diet. Expression of mRNAs was normalized to Gusb and Hprt mRNA and set to unity in wild-type controls. (**g**) Representative western-blot analysis of in vitro phosphorylation of c-Jun (p-c-Jun) in liver and skeletal muscle (SM) lysates from miR-143–145 knockout mice ($n = 4$) and wild-type controls ($n = 4$) on a high-fat diet. Immunoreactive phospho-c-Jun was normalized to total JNK input and the quotient of wild-type controls was set to unity. All error bars indicate s.e.m. $*P \leq 0.05$, $**P \leq 0.01$, $***P \leq 0.001$. Uncropped images of blots are shown in Supplementary Fig. S9.

tumour-necrosis factor-α (Tnf-α) was unaltered in white adipose tissue of miR-143–145-deficient mice (Fig. 6f). Activation of inflammatory

signalling cascades such as c-Jun N-terminal kinase (JNK) signalling in liver and skeletal muscle has been demonstrated to be critical in the

development of insulin resistance; we therefore directly determined JNK activity in these tissues, but did not detect significant differences between miR-143–145-deficient and control mice (Fig. 6g).

Thus, miR-143–145 deficiency *in vivo* protects from diet-induced inhibition of AKT activation and partly restores diet-induced deterioration of glucose metabolism in the absence of altered adipose-tissue mass, macrophage infiltration or systemic JNK activation, substantiating that increased expression of miR-143 critically contributes to obesity-induced insulin resistance.

In vivo SILAC identifies ORP8 as an miR-143 target

To identify the molecular target(s) of miR-143 in the development of insulin resistance, we next employed *in vivo* stable isotope labelling of amino acids (SILAC; ref. 29) for quantitative-mass-spectrometry-based analysis of hepatic protein expression in miR-143[DOX] mice. Protein lysates extracted from hepatocytes of doxycycline-treated miR-143[DOX] and control mice were mixed 1:1 with extracts of primary hepatocytes from mice that had been labelled with $^{13}C_6$-lysine *in vivo* (SILAC mice). Mixing lysates of control mice with SILAC lysates and mixing SILAC lysates with miR-143[DOX] lysates allowed for indirect comparison of protein expression between miR-143[DOX] and control mice (Fig. 7a). Independent processing of two samples from miR-143[DOX] and control mice enabled us to determine the relative abundance of 2,043 proteins. Of these, peptide fragments of 1,463 proteins were detectable in both experiments (72% overlap), of which 214 proteins were upregulated and 48 were downregulated by 25% or more in liver extracts of miR-143[DOX] when compared with control mice (see Supplementary Table S3).

In an attempt to identify *bona fide* targets undergoing miR-143-dependent post-transcriptional silencing, we analysed the proteins downregulated on miR-143 overexpression for predicted miR-143 binding sites in their 3′ untranslated region (UTR). Five proteins exhibited predicted 3′-UTR binding sites for miR-143, and one of them—namely ORP8—had three predicted miR-143 binding sites (see Supplementary Table S4).

The functional significance of the predicted ORP8 3′-UTRmiR-143-interaction sites was tested employing luciferase reporter assays. Overexpressed intact miR-143 target sites, but not mutant miR-143 target sites, were able to mediate repression of reporter-gene activity (Fig. 7b). Repression of reporter-gene activity was most efficiently reversed on mutation of target site 1, and mutation of all three binding sites resulted in a significant twofold increase in luciferase activity. These data indicate that all three binding sites of miR-143 in the 3′ UTR of ORP8 cooperatively confer repression of reporter-gene activity.

Analysis of hepatic ORP8 expression confirmed a significant downregulation of ORP8 protein expression by 50% in miR-143[DOX] mice when compared with controls (Fig. 7c), whereas *Orp8* mRNA expression remained unaltered (Fig. 7d). Conversely, hepatic ORP8 expression in miR-143–145-deficient mice was increased 1.9-fold when compared with controls (Fig. 7e), again in the absence of significant alterations of *Orp8* mRNA expression (Fig. 7f). Taken together, these approaches revealed ORP8 as a target for miR-143-dependent post-transcriptional gene silencing.

ORP8 promotes insulin-stimulated AKT activation

ORP8 is expressed at high levels in macrophages[30], followed by substantial expression in liver and brain and little or no expression in heart, skeletal muscle and white adipose tissue (Fig. 8a). ORP8 binds 25-OH-cholesterol, which in turn has been shown to regulate AKT signalling during apoptosis by promoting proteasomal degradation of AKT and/or inhibition of PI(3)K in macrophages[31,32]. To directly investigate a potential role for ORP8 in control of insulin-stimulated AKT activation, we analysed AKT phosphorylation in insulin-stimulated HepG2 cells transfected with short interfering RNAs (siRNAs) directed to human ORP8 (*Orp8* siRNAs). Western-blot analysis revealed successful reduction of ORP8 protein expression by 80% or more in cells transfected with *Orp8* siRNAs, whereas no reduction was detected in cells transfected with control siRNAs (Fig. 8b). Interestingly, insulin-stimulated AKT activation and consistently phosphorylation of the AKT substrate glycogen synthase kinase 3β (GSK3β) were reduced in ORP8-depleted cells (Fig. 8c).

To further substantiate the requirement of ORP8 expression for ability of insulin to stimulate AKT phosphorylation, we generated immortalized murine liver cells that stably express two different shRNAs directed to murine ORP8 (*Orp8* shRNA) or a control shRNA. Western-blot analysis confirmed that the clones expressing either of the *Orp8* shRNAs exhibited greatly reduced ORP8 expression (Fig. 8d). Moreover, these cells exhibited a significant reduction of insulin-stimulated AKT activation (Fig. 8e,f). Consistent with impaired AKT activation, insulin-stimulated phosphorylation of the AKT target, the forkhead O-family (FOXO) transcription factors, was also significantly impaired in ORP8-depleted cells (Fig. 8e,g). Taken together, our results indicate that OPR8 affects insulin's ability to regulate AKT phosphorylation and downstream kinase signalling in liver cells.

DISCUSSION

Our finding that miR-143–145 expression is dysregulated in *db/db* mice is consistent with other studies describing miR-143 as being up- or downregulated in tissues of *ob/ob* (refs 28,33), diet-induced obese[33,34] and diabetic mice[35] as well as human patients[36]. At present it is unclear whether differences in genetic background, diet composition or miRNA-detection methods account for the variable findings with respect to miR-143 expression in adipose tissue[28,33,34] and liver[35] of these models.

However, the physiological relevance of dysregulated miR-143 expression in obesity has remained elusive so far. Studies addressing the role of miR-143 in adipose tissue by gain- or loss-of-function approaches provided evidence for an adipocyte-differentiation-promoting effect of miR-143 *in vitro*[28,33]. In contrast, our studies in miR-143–145-deficient mice reveal that both miRNAs seem to be dispensable for adipose-tissue formation and maintenance *in vivo*. Nevertheless, our finding of increased hepatic miR-143 expression in two different obesity mouse models and the discovery that miR-143 affects hepatic insulin action and systemic glucose homeostasis *in vivo*, as independently demonstrated by overexpression and knockout mouse models, characterize miR-143 as an integrator of metabolic signalling. This provides functional evidence for a role of altered post-transcriptional gene silencing in the development of obesity-associated insulin resistance *in vivo*.
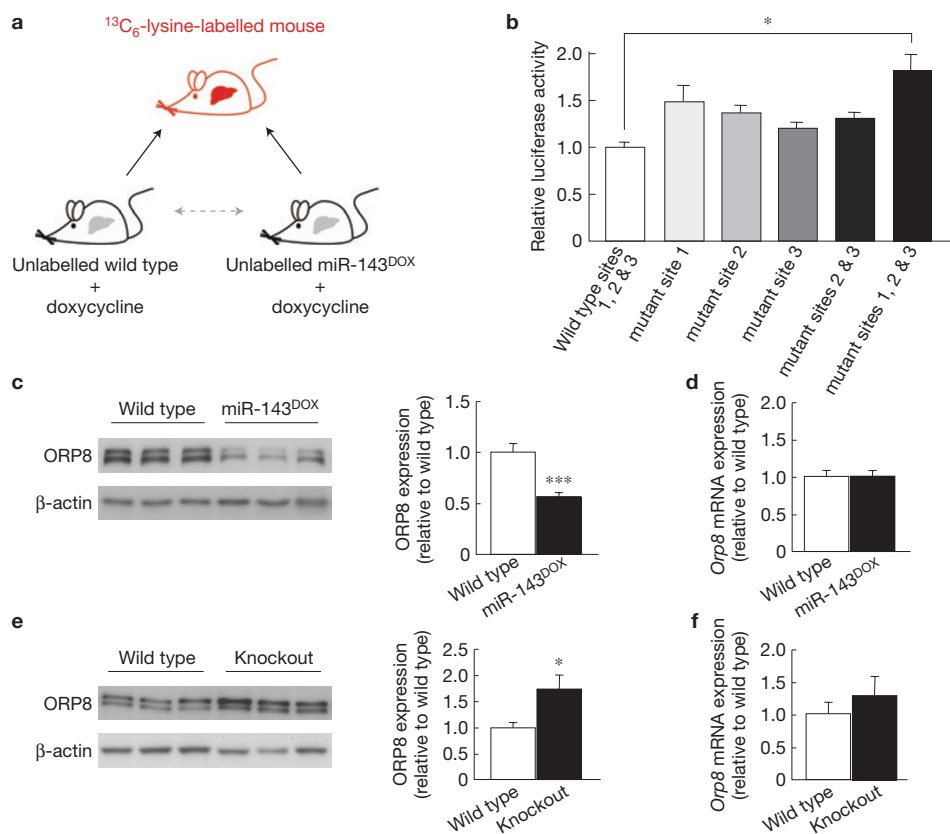
Figure 7 *In vivo* SILAC identifies ORP8 as an miR-143 target. (**a**) General scheme of the *in vivo* SILAC approach. Protein expression in the liver of $^{13}C_6$-lysine-labelled (SILAC) mice was analysed and compared with doxycycline-treated unlabelled wild-type and miR-143^{DOX} mice, respectively. Differences in protein expression between SILAC and miR-143^{DOX} mice were normalized for the ratio SILAC/unlabelled wild type, thus allowing for indirect comparison of protein expression between miR143^{DOX} mice and wild-type littermate controls. (**b**) Relative luciferase activity of the indicated reporter constructs. Firefly luciferase activity was normalized to the activity of co-expressed *Renilla* luciferase. Luciferase activity of the reporter construct, containing the wild-type miR-143 binding sites to ORP8 (open bar), was set to unity. Results represent five independent experiments. All error bars indicate s.e.m. $*P \leq 0.05$. (**c**) Representative western-blot analysis of ORP8 expression in the liver of miR-143^{DOX} mice ($n = 12$) and wild-type littermate controls ($n = 12$). β-actin was used as a loading control. (**d**) Real-time PCR analysis of *Orp8* mRNA expression in the liver of miR-143^{DOX} mice ($n = 11$), compared with wild-type controls ($n = 14$). Expression of mRNAs was normalized to *Gusb* and *Hprt* mRNA. (**e**) Representative western-blot analysis of ORP8 expression in the liver of miR-143–145 knockout mice ($n = 9$) and wild-type littermate controls ($n = 9$). miR-143–145 knockout mice but not miR-143^{DOX} mice were on a high-fat diet. β-actin was used as a loading control. (**f**) Real-time PCR analysis of *Orp8* mRNA expression in the liver of miR-143–145 knockout mice ($n = 6$), compared with wild-type controls ($n = 6$), on a high-fat diet. Expression of mRNAs was normalized to *Gusb* and *Hprt* mRNA. For western-blot and real-time PCR analysis ORP8 expression in wild-type controls was set to unity. All error bars indicate s.e.m. $*P \leq 0.05$, $***P \leq 0.001$. Uncropped images of blots are shown in Supplementary Fig. S9.

One important area of future research will be to define the molecular mechanisms leading to hepatic miR-143 overexpression in obesity. Interestingly, the putative promoter region of the miR-143–145 cluster contains numerous predicted consensus binding sites for FOXO transcription factors, which are inactivated in an insulin–PI(3)K–AKT-dependent manner and represent transcriptional regulators of key metabolic pathways[37,38]. Thus, we propose the existence of an autoregulatory loop, in which obesity-induced insulin resistance, through FOXO-dependent upregulation of hepatic miR-143 expression, propagates a feedback mechanism that further inhibit insulin action in an miR-143–ORP8-dependent manner.

As we also find miR-145 to be dysregulated in obesity, but do not detect alterations in glucose metabolism in mice overexpressing miR-145, a potential role of this miRNA in other aspects of obesity-induced metabolic deteriorations needs to be further elucidated. Recent studies have defined a pivotal role for miR-143 in cooperation with miR-145 in control of vascular homeostasis by regulating smooth-muscle cell fate and plasticity[39,40] or the responsiveness of angiotensin-converting enzyme (ACE), which affects both the synthetic phenotype and contractile functions of smooth muscle cells[23]. Therefore, obesity-associated dysregulation of miR-143–145 might also provide a link between obesity, increased cardiovascular risk and impaired blood-pressure control and thus represents a potential therapeutic target[41]. However, reduced expression of miR-143–145 has been described in various cancer types, for example colorectal cancer[42,43], B-cell malignancies[44] and prostate cancer[45], warranting caution when considering targeting these miRNAs for treatment of metabolic disorders.

The present study further provides evidence for miR-143–ORP8-dependent regulation of AKT signalling, which, as well as its central role in energy metabolism, coordinates diverse biological processes ranging from cell growth and differentiation to carcinogenesis[46,47]. Our experiments reveal impaired insulin-stimulated AKT activation on miR-143 overexpression and ORP8 downregulation without
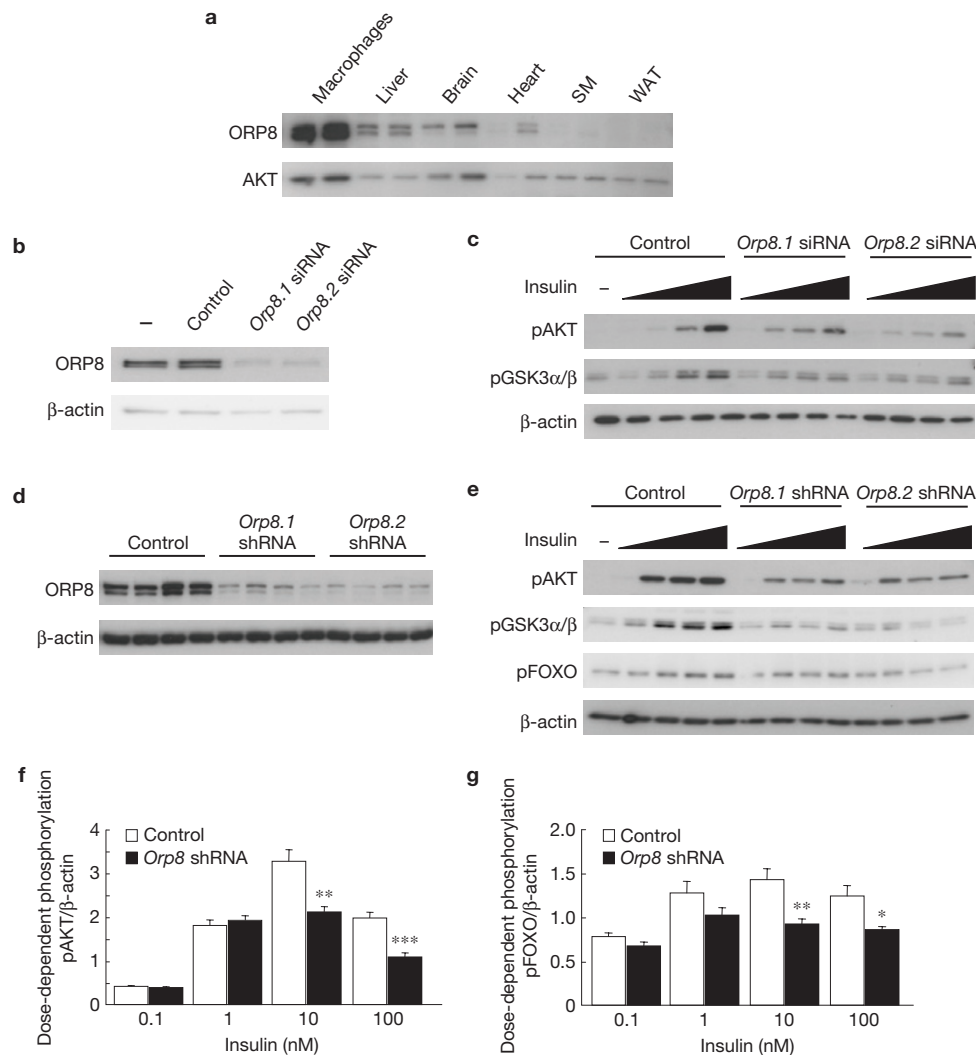
Figure 8 Downregulation of ORP8 in cultured liver cells impairs insulin-stimulated AKT activation. (**a**) Western-blot analysis of ORP8 expression in the indicated tissues of wild-type C57BL/6 mice. AKT was used as a loading control. (**b**) Western-blot analysis of ORP8 expression in HepG2 cells transfected with the indicated siRNA oligonucleotides. β-actin was used as a loading control. (**c**) Western-blot analysis of insulin-stimulated phosphorylation of AKT and GSK3 in HepG2 cells transfected with the indicated siRNA oligonucleotides. β-actin was used as a loading control. Serum-depleted cells were stimulated with either saline (−) or increasing concentrations of insulin (0.1–100 nM). (**d**) Western-blot analysis of ORP8 expression in retroviral-transformed Hepa1–6 cell clones stably expressing the indicated shRNA. β-actin was used as a loading control. (**e**) Representative western-blot analysis of insulin-stimulated phosphorylation of AKT, GSK3 and FOXO levels in Hepa1–6 cell clones stably expressing the indicated shRNA. β-actin was used as a loading control. Serum-depleted cells were stimulated with either saline (−) or increasing concentrations of insulin (0.1–100 nM). (**f**) Quantification of dose-dependent insulin-stimulated AKT phosphorylation. Protein expression was quantified in six independent control-shRNA- and Orp8-shRNA-expressing Hepa1–6 cell clones. Relative values represent the average of three independent experiments for each clone. (**g**) Quantification of dose-dependent insulin-stimulated FOXO phosphorylation. Protein expression was quantified in six independent control-shRNA- and Orp8-shRNA-expressing Hepa1–6 cell clones. Relative values represent the average of three independent experiments for each clone. All error bars indicate s.e.m. $*P \leq 0.05, **P \leq 0.01, ***P \leq 0.001$. Uncropped images of blots are shown in Supplementary Fig. S9.

an impact on insulin receptor–IRS-1 activation, indicating that ORP8 acts closely upstream of or directly at AKT phosphorylation. Although previous work in haematopoetic cells has demonstrated that 25-OH cholesterol, an ORP8 ligand, inhibits AKT signalling through induction of AKT degradation[48], we find that in hepatocytes 25-OH-cholesterol-dependent inhibition of insulin-stimulated AKT activation occurs in the absence of altered AKT expression, arguing for an extra regulatory mechanism of oxysterol-dependent AKT inhibition in liver. However, the exact mechanism of ORP8-mediated AKT inhibition remains enigmatic at this point, as do the functions of ORPs in general.

ORPs act as sterol sensors that relay information to diverse cellular processes such as intracellular sterol transport, integration of sterol and sphingomyelin metabolism, regulation of neutral lipid metabolism, secretory vesicle generation and microtubule-based motility of endo-lysosomes[49]. A direct oxysterol-dependent regulation of kinase activity has been revealed for oxysterol-binding protein (OSBP)—the 'founding member' of the ORP family. OSBP interacts with a member of the PTPPBS (protein tyrosine phosphatase (PC12, Br7, Sl)) family of tyrosine phosphatases, the serine–threonine phosphatase protein phosphatase 2 (PP2A) and cholesterol to regulate extracellular signal-regulated kinase (ERK) phosphorylation. When exposed to oxysterols

or on low cellular cholesterol levels, the oligomer disassembles and ERK phosphorylation increases[50]. As PP2A activity represents an important regulator of AKT activation[51], we are at present investigating the possibility of an oxysterol-ORP8-dependent regulation of AKT phosphatases. In addition, we cannot rule out the existence of further miR-143 target(s) that regulate insulin- and AKT-dependent signalling and still await identification.

Our study also provides general technical advances in studying miRNA function *in vivo*. Given the pleiotropic roles of miRNAs in developmental processes, the establishment of a generally applicable technology to conditionally overexpress miRNAs in transgenic mice provides an important tool for miRNA research. Further adaptations of the expression system, such as inclusion of a *loxP*-flanked stop-cassette in the H1 promoter, will further enable inducible tissue-specific miRNA expression[52].

The combination of inducible miRNA overexpression in mice with SILAC-based quantitative mass spectrometry enabled us to identify ORP8 as an miR-143 target regulated at the level of mRNA translation, further underlining large-scale protein quantification as an indispensable tool to unravel miRNA targets.

Our present study has identified an miR-143-controlled ORP8-dependent regulatory pathway of AKT signalling in obesity and thus sets the stage to develop miR-143, ORP8 and potentially other miR-143 target genes as future therapeutic targets for obesity-associated insulin resistance, diabetes and other obesity-associated diseases. □

METHODS

Methods and any associated references are available in the online version of the paper at http://www.nature.com/naturecellbiology/

Note: Supplementary Information is available on the Nature Cell Biology website

AUTHOR CONTRIBUTIONS

S.D.J. and J.C.B. designed the research; S.D.J. carried out most of the experiments; M.K. carried out *in vivo* SILAC analyses; D.M.W. and N.R. provided extra technical assistance; F.T.W. helped to design cloning strategies; H.S.B. analysed energy expenditure in miR-143[DOX] mice; C.M. carried out luciferase assays; H.K. helped with lentivirus experiments; V.M.O. provided ORP8 antibody and shRNA ORP8 lentiviruses. T. Böttger and T. Braun provided miR143–145 knockout mice; J.S. in part generated miR-143[DOX] and miR-145[DOX] mice and provided *LacZ* shRNA[DOX] mice. S.D.J. and J.C.B. wrote the manuscript. All authors participated in the interpretation of the data and production of the final manuscript.

COMPETING FINANCIAL INTERESTS

The authors declare no competing financial interests.

Published online at http://www.nature.com/naturecellbiology

Reprints and permissions information is available online at http://npg.nature.com/reprintsandpermissions/

1. Mokdad, A. H. *et al.* The continuing increase of diabetes in the US. *Diabetes Care* **24**, 412 (2001).
2. Froguel, P., Velho, G., Passa, P. & Cohen, D. Genetic determinants of type 2 diabetes mellitus: lessons learned from family studies. *Diabete Metab.* **19**, 1–10 (1993).
3. Bruning, J. C. *et al.* Development of a novel polygenic model of NIDDM in mice heterozygous for IR and IRS-1 null alleles. *Cell* **88**, 561–572 (1997).
4. Martin, B. C. *et al.* Role of glucose and insulin resistance in development of type 2 diabetes mellitus: results of a 25-year follow-up study. *Lancet* **340**, 925–929 (1992).
5. Kahn, C. R. Banting Lecture. Insulin action, diabetogenes, and the cause of type II diabetes. *Diabetes* **43**, 1066–1084 (1994).
6. Moller, D. E., Yokota, A., White, M. F., Pazianos, A. G. & Flier, J. S. A naturally occurring mutation of insulin receptor alanine 1134 impairs tyrosine kinase function and is associated with dominantly inherited insulin resistance. *J. Biol. Chem.* **265**, 14979–14985 (1990).
7. Almind, K. *et al.* Aminoacid polymorphisms of insulin receptor substrate-1 in non-insulin-dependent diabetes mellitus. *Lancet* **342**, 828–832 (1993).
8. George, S. *et al.* A family with severe insulin resistance and diabetes due to a mutation in AKT2. *Science* **304**, 1325–1328 (2004).
9. Puig, O. & Tjian, R. Transcriptional feedback control of insulin receptor by dFOXO/FOXO1. *Genes Lancet Dev.* **19**, 2435–2446 (2005).
10. Aguirre, V., Uchida, T., Yenush, L., Davis, R. & White, M. F. The c-Jun NH(2)-terminal kinase promotes insulin resistance during association with insulin receptor substrate-1 and phosphorylation of Ser(307). *J. Biol. Chem.* **275**, 9047–9054 (2000).
11. Zhande, R., Mitchell, J. J., Wu, J. & Sun, X. J. Molecular mechanism of insulin-induced degradation of insulin receptor substrate 1. *Mol. Cell Biol.* **22**, 1016–1026 (2002).
12. Lagos-Quintana, M., Rauhut, R., Lendeckel, W. & Tuschl, T. Identification of novel genes coding for small expressed RNAs. *Science* **294**, 853–858 (2001).
13. Lau, N. C., Lim, L. P., Weinstein, E. G. & Bartel, D. P. An abundant class of tiny RNAs with probable regulatory roles in *Caenorhabditis elegans*. *Science* **294**, 858–862 (2001).
14. Lee, R. C. & Ambros, V. An extensive class of small RNAs in *Caenorhabditis elegans*. *Science* **294**, 862–864 (2001).
15. Lee, R. C., Feinbaum, R. L. & Ambros, V. The *C. elegans* heterochronic gene lin-4 encodes small RNAs with antisense complementarity to lin-14. *Cell* **75**, 843–854 (1993).
16. Xu, P., Vernooy, S. Y., Guo, M. & Hay, B. A. The *Drosophila* microRNA Mir-14 suppresses cell death and is required for normal fat metabolism. *Curr. Biol.* **13**, 790–795 (2003).
17. Poy, M. N. *et al.* A pancreatic islet-specific microRNA regulates insulin secretion. *Nature* **432**, 226–230 (2004).
18. Poy, M. N., Spranger, M. & Stoffel, M. microRNAs and the regulation of glucose and lipid metabolism. *Diabetes Obes. Metab.* **9** (Suppl 2), 67–73 (2007).
19. Saxena, R. *et al.* Genome-wide association analysis identifies loci for type 2 diabetes and triglyceride levels. *Science* **316**, 1331–1336 (2007).
20. Scott, L. J. *et al.* A genome-wide association study of type 2 diabetes in Finns detects multiple susceptibility variants. *Science* **316**, 1341–1345 (2007).
21. Coleman, D. L. Obese and diabetes: two mutant genes causing diabetes-obesity syndromes in mice. *Diabetologia* **14**, 141–148 (1978).
22. Chen, H. *et al.* Evidence that the diabetes gene encodes the leptin receptor: identification of a mutation in the leptin receptor gene in *db/db* mice. *Cell* **84**, 491–495 (1996).
23. Boettger, T. *et al.* Acquisition of the contractile phenotype by murine arterial smooth muscle cells depends on the Mir143/145 gene cluster. *J. Clin. Invest.* **119**, 2634–2647 (2009).
24. Gangaraju, V. K. & Lin, H. MicroRNAs: key regulators of stem cells. *Nat. Rev. Mol. Cell Biol.* **10**, 116–125 (2009).
25. Seibler, J. *et al.* Reversible gene knockdown in mice using a tight, inducible shRNA expression system. *Nucleic Acids Res.* **35**, e54 (2007).
26. Koch, L. *et al.* Central insulin action regulates peripheral glucose and fat metabolism in mice. *J. Clin. Invest.* **118**, 2132–2147 (2008).
27. Leavens, K. F., Easton, R. M., Shulman, G. I., Previs, S. F. & Birnbaum, M. J. Akt2 is required for hepatic lipid accumulation in models of insulin resistance. *Cell Metab.* **10**, 405–418 (2009).
28. Esau, C. *et al.* MicroRNA-143 regulates adipocyte differentiation. *J. Biol. Chem.* **279**, 52361–52365 (2004).
29. Kruger, M. *et al.* SILAC mouse for quantitative proteomics uncovers kindlin-3 as an essential factor for red blood cell function. *Cell* **134**, 353–364 (2008).
30. Yan, D. *et al.* OSBP-related protein 8 (ORP8) suppresses ABCA1 expression and cholesterol efflux from macrophages. *J. Biol. Chem.* **283**, 332–340 (2008).
31. Rusinol, A. E. *et al.* AKT/protein kinase B regulation of BCL family members during oxysterol-induced apoptosis. *J. Biol. Chem.* **279**, 1392–1399 (2004).
32. Vejux, A. *et al.* Phospholipidosis and down-regulation of the PI3-K/PDK-1/Akt signalling pathway are vitamin E inhibitable events associated with 7-ketocholesterol-induced apoptosis. *J. Nutr. Biochem.* **20**, 45–61 (2009).
33. Xie, H., Lim, B. & Lodish, H. F. MicroRNAs induced during adipogenesis that accelerate fat cell development are downregulated in obesity. *Diabetes* **58**, 1050–1057 (2009).
34. Takanabe, R. *et al.* Up-regulated expression of microRNA-143 in association with obesity in adipose tissue of mice fed high-fat diet. *Biochem. Biophys. Res. Commun.* **376**, 728–732 (2009).
35. Li, S. *et al.* Differential expression of microRNAs in mouse liver under aberrant energy metabolic status. *J. Lipid Res.* **50**, 1756–1765 (2009).
36. Gallagher, I.J. *et al.* Integration of microRNA changes *in vivo* identifies novel molecular features of muscle insulin resistance in type 2 diabetes. *Genome Med.* **2**, 9 (2010).

37. Brunet, A. *et al.* Akt promotes cell survival by phosphorylating and inhibiting a Forkhead transcription factor. *Cell* **96,** 857–868 (1999).

38. Accili, D. & Arden, K. C. FoxOs at the crossroads of cellular metabolism, differentiation, and transformation. *Cell* **117,** 421–426 (2004).

39. Cordes, K. R. *et al.* miR-145 and miR-143 regulate smooth muscle cell fate and plasticity. *Nature* **460,** 705–710 (2009).

40. Xin, M. *et al.* MicroRNAs miR-143 and miR-145 modulate cytoskeletal dynamics and responsiveness of smooth muscle cells to injury. *Genes Dev.* **23,** 2166–2178 (2009).

41. Zhou, L. *et al.* Prevalence, incidence and risk factors of chronic heart failure in the type 2 diabetic population: systematic review. *Curr. Diabetes Rev.* **5,** 171–184 (2009).

42. Michael, M. Z., SM, O. C., van Holst Pellekaan, N. G., Young, G. P. & James, R. J. Reduced accumulation of specific microRNAs in colorectal neoplasia. *Mol. Cancer Res.* **1,** 882–891 (2003).

43. Slaby, O. *et al.* Altered expression of miR-21, miR-31, miR-143 and miR-145 is related to clinicopathologic features of colorectal cancer. *Oncology* **72,** 397–402 (2007).

44. Akao, Y., Nakagawa, Y., Kitade, Y., Kinoshita, T. & Naoe, T. Downregulation of microRNAs-143 and -145 in B-cell malignancies. *Cancer Sci.* **98,** 1914–1920 (2007).

45. Clape, C. *et al.* miR-143 interferes with ERK5 signaling, and abrogates prostate cancer progression in mice. *PLoS One* **4,** e7542 (2009).

46. Whiteman, E. L., Cho, H. & Birnbaum, M. J. Role of Akt/protein kinase B in metabolism. *Trends Endocrinol. Metab.* **13,** 444–451 (2002).

47. Toker, A. & Yoeli-Lerner, M. Akt signaling and cancer: surviving but not moving on. *Cancer Res.* **66,** 3963–3966 (2006).

48. Liu, J., Netherland, C., Pickle, T., Sinensky, M. S. & Thewke, D. P. Stimulation of Akt poly-ubiquitination and proteasomal degradation in P388D1 cells by 7-ketocholesterol and 25-hydroxycholesterol. *Arch. Biochem. Biophys.* **487,** 54–58 (2009).

49. Olkkonen, V. M. *et al.* The OSBP-related proteins (ORPs): global sterol sensors for co-ordination of cellular lipid metabolism, membrane trafficking and signalling processes? *Biochem. Soc. Trans.* **34,** 389–391 (2006).

50. Wang, P. Y., Weng, J. & Anderson, R. G. OSBP is a cholesterol-regulated scaffolding protein in control of ERK 1/2 activation. *Science* **307,** 1472–1476 (2005).

51. Ugi, S. *et al.* Protein phosphatase 2A negatively regulates insulin's metabolic signaling pathway by inhibiting Akt (protein kinase B) activity in 3T3-L1 adipocytes. *Mol. Cell Biol.* **24,** 8778–8789 (2004).

52. Ventura, A. *et al.* Cre-lox-regulated conditional RNA interference from transgenes. *Proc. Natl Acad. Sci. USA* **101,** 10380–10385 (2004).

METHODS

Animal care. Care of all animals was within institutional animal-care committee guidelines, and all procedures were approved by local government authorities (Bezirksregierung Köln) and were in accordance with NIH guidelines. Mice were housed in groups of three to five at 22–24 °C using a 12 h light–12 h dark cycle with lights on at 06:00. Unless otherwise stated, animals were fed normal chow diet (Teklad Global Rodent no. T.2018.R12; Harlan). Eight-week-old doxycycline-inducible transgenic mice and C57BL/6 littermates (wild type) were administered drinking water supplemented with 10% sucrose (AppliChem) plus 4 mg ml^{-1} doxycycline hyclate (Sigma-Aldrich) for 4 weeks unless stated otherwise. Doxycycline-supplemented water was protected from light and changed every 2 days. The animals had *ad libitum* access to water at all times, and food was only withdrawn if required for an experiment. Diet-induced obesity was obtained by feeding a high-fat diet (no. C1057; Altromin) containing 32.7% carbohydrates, 20% protein and 35.5% fat (55.2% of calories from fat) for at least 8 weeks.

Cloning of small RNA molecules. Total RNA (600 µg) isolated from the liver was separated on a 15% (w/v) denaturing polyacrylamide gel. A total of 19–24 nucleotide small RNAs were recovered from the gel and used as input for adaptor ligation. Adaptor ligation and PCR with reverse transcription (RT–PCR) of the ligation product (5′ RT–PCR primer first PCR 5′-CAGCCAACGGAATTCCTCACTAAA-3′; 3′ RT–PCR primer first PCR 5′-GACTAGCTTGGTGCCGAATCGCGGTTAAA-3′; 5′ RT–PCR primer second PCR 5′-GAGCCAACAGGCCCGAATTCCTCACTAAA-3′; 3′ RT–PCR primer second PCR 5′-GACTAGCTTGGTGCCGAATCGCGGTTAAA-3′) was carried out as described in *Current Protocols in Molecular Biology*[53]. Concatamers containing isolated small RNAs flanked by adapter sequences were cloned into the pCR2.1 vector (Invitrogen) and automatically sequenced using M13 F primer 5′-GTAAAACGACGGCCAG-3′ (MWG).

Northern-blot analysis. Indicated tissues were dissected and homogenized in peqGOLD TriFast solution (peqLab) with a polytron homogenizer (IKA Werke). RNA was isolated according to the manufacturer's instructions, separated on a 15% denaturing polyacrylamide gel and electroblotted on a nylon membrane (Perkin Elmer). [γ-^{32}P]ATP end-labelled (NEB) oligonucleotide probes (MWG) for mature miRNAs (mmu-miR-143 5′-TGAGCTACAGTGCTTCATCTCA-3′, mmu-miR-145 5′-AGGGATTCCTGGGAAAACTGGAC-3′) were hybridized to the membrane overnight at 50 °C. Equal loading was verified using a probe for 5S ribosomal RNA (5′-TCCTGCAATTCACATTAATTCTCGCAGCTAGC-3′).

TaqMan real-time quantitative RT-PCR. Measurements of mature miRNA levels by quantitative real-time PCR were made using a TaqMan microRNA RT Kit and TaqMan MicroRNA Assays (Applied Biosystems) according to the manufacturer's instructions. mRNA levels were determined using EuroScript Reverse Transcriptase (Eurogentec) and TaqMan Assay on Demand kits (Applied Biosystems) according to the manufacturer's instructions. Relative expression of mature miRNAs and mRNAs was determined using a comparative method ($2^{-\delta\delta CT}$) according to the ABI Relative Quantification Method. Assays were linear over four orders of magnitude.

Generation of miR-143^{DOX} mice. Mice overexpressing miR-143 were generated similarly to previously described shRNA-expressing mice[25]. The miR-143 coding region flanked by about 200 base pairs (bp) of the endogenous locus was PCR-amplified from mouse genomic DNA using the primers 5Xba_143_H1 5′-AAATCTAGAAGCCAAGACCCGGATAGGA-3′ and 3Xho_143_H1 5′-AAACTCGAGAAAAACAAGCTGCTGGAGCAGAATC-3′. Correct recombinase-mediated cassette exchange (RMCE) in embryonic stem cells was confirmed by Southern-blot analysis using a standard protocol. Genomic DNA was digested with HindIII. The validated embryonic stem cells were injected into F1 blastocytes as previously described[25]. Doxycycline-treated miRNA mice are referred to as miR-143^{DOX} and doxycycline-treated C57BL/6 littermates as wild type.

Body temperature and indirect calorimetry. Body temperature was determined anally on three consecutive days at 10:00 using a TH-5 Monitoring Thermometer (Physitemp Intruments). Indirect calorimetry measurements were made in a PhenoMaster System (TSE systems). Mice were placed at room temperature (22–24 °C) in 7.1 l chambers of the PhenoMaster open-circuit calorimetry. Mice were allowed to adapt to the chambers for at least 24 h. Food and water were provided *ad libitum* in the appropriate devices. Parameters of indirect calorimetry were measured for at least the following 48 h.

Analytical procedures. Blood glucose values were determined from whole venous blood using an automatic glucose monitor (GlucoMen GlycÓ; A. Menarini Diagnostics). Serum insulin and leptin levels were measured by enzyme-linked immunosorbent assay using mouse standards according to the manufacturer's guidelines (Mouse–Rat Insulin ELISA, Mouse Leptin ELISA, Crystal Chem).

Glucose- and insulin-tolerance tests. Glucose-tolerance tests were carried out on animals that had been fasted overnight for 16 h as previously described[54]. After determination of fasted blood glucose levels, each animal received an intraperitoneal (i.p.) injection of 2 g/kg body weight of glucose (20% glucose; Delta Select). Blood glucose levels were detected after 15, 30, 60 and 120 min. Insulin-tolerance tests were carried out on random-fed animals. After determination of random-fed blood glucose levels, each animal received an i.p. injection of 0.75 U kg^{-1} body weight of insulin (Actrapid; Novo Nordisk). Blood glucose levels were detected after 15, 30 and 60 min.

Glucose-stimulated insulin secretion. All animals were fasted overnight for 16 h. Blood samples were collected from mice before an i.v. injection of 2 mg g^{-1} body weight of glucose (20% glucose; Delta Select). Further blood samples were collected 2, 5, 15, 30 and 60 min after the injection and serum insulin levels were determined.

Immunohistochemistry. Pancreatic tissue was excised, snap-frozen and sliced as previously described[26]. Haematoxylin and eosin, insulin and glucagon stainings were carried out as previously described[26]. Stainings were analysed with a Zeiss Axioskop 40 microscope (Carl Zeiss MicroImaging) and cell mass was determined using Zeiss AxioVision 4.2 software (Carl Zeiss MicroImaging). Dissected white- and brown-adipose-tissue samples were incubated in fixation solution containing 4% paraformaldehyde at 4 °C overnight, embedded in paraffin and sliced according to a previously described standard protocol[55]. Haematoxylin and eosin staining, Mac-2 and UCP-1 immunohistochemistry were carried out after deparaffinization as previously described[55,56].

Insulin signalling. After an overnight fast, mice were anaesthetized and the abdominal cavity of the mice was opened to inject either 5 units normal human insulin (Actrapid; Novo Nordisk 40 U ml^{-1}) or insulin diluent, diluted in 0.9% saline (final volume 125 µl) into the *vena cava inferior*. Samples of liver and skeletal muscle were collected 2 and 5 min after injection respectively, and proteins were extracted from tissues for western-blot analysis.

Western-blot analysis. Indicated tissues were dissected and homogenized in lysis buffer using a Polytron homogenizer (IKA Werke) as previously described[54]. Western-blot analyses were carried out according to standard protocols with antibodies raised against IR-β (no. sc-711, Santa Cruz Biotechnology, 1:200), pIR (no. CSA-720, Stressgen, 1:500), AKT (no. 9,272, Cell Signaling, 1:1,000), phosphoAKT Ser 473 (no. 9,271, Cell Signaling, 1:1,000), phosphoAKT Thr 308 (no. 4,056, Cell Signaling, 1:1,000), p85 (no. 06-195, Upstate, 1:5,000), p44/42 (ERK1/2) (no. 9,102, Cell Signaling, 1:1,000) and ORP8 (1:1,000; ref. 30). β-actin (no. A5441, Sigma,1:5,000) and α-tubulin (no. T6074, Sigma, 1:5,000) were used as loading controls. JNK activity was determined using a KinasEeSTAR JNK activity assay kit (no. K431-40, BioVision) according to the manufacturer's instructions.

***In vivo* SILAC.** Quantitative-mass-spectrometry analysis was carried out as previously described[29]. Raw data files were converted to Mascot generic format files with in-house software (Raw2MSM), and Mascot (version 2.0) was used for database search and protein identification. Only proteins that had at least two peptides with ion scores higher than 20 were considered for identification and quantification. MSQuant was used to verify and quantify the resulting SILAC-peptide pairs. A target decoy database approach was used to identify false-positive peptides and to set threshold criteria such that fewer than 1% of false positives were included. Samples were analysed by the software MaxQuant, which carries out a peak list, SILAC- and extracted ion chromatography-based quantification, false-positive rates and peptide identification on the basis of Mascot search results. All data were searched against the International Protein Index sequence database (mouse International Protein Index, version 3.24; ref. 29).

Expression microarrays. Biotin-labelled complementary DNA was synthesized using GeneChip Whole Transcript Sense Target Labelling Assay (Affymetrix) according to the manufacturer's instructions. Following fragmentation, complementary DNAs were hybridized for 17 h at 45 °C on Affymetrix Mouse Gene 1.0 ST Arrays. Arrays were washed and stained in the GeneChip Fluidics Station 450 (Affymetrix) and scanned on a GeneChip Scanner 3000 7G (Affymetrix). Data intensities were log-transformed and normalized with a quantile normalization method using Partek Genomics Suite.

Database accession numbers. Microarray experiments complied with MIAME (minimum information about microarray experiments) and are available through the public repository Gene Expression Ominibus (GEO) at accession number GSE26460.

Cell culture. For RNA interference experiments, HepG2 cells were transfected with 100 pmol human ORP8-specific (*Orp8.1* siRNA 5′-GGAGCUUGGUGGAACAG-UCAAUAUU-3′, *Orp8.2* siRNA 5′-GAAGCACGGUUAACUUUCUUGAAUA-3′) or scrambled control siRNAs (lowGC) (Invitrogen) using Lipofectamine 2000 (Invitrogen) according to the manufacturer's instructions. Stable murine shRNA liver cell lines were generated using MISSION non-target shRNA (5′-CCGGCAACAAGATGAAGAGCACCAACTCGAGTTGGTGCTCTTCATCTTG-TTGTTTTT-3′) and *Orp8* shRNA transduction particles (*Orp8.1* shRNA loop sequence 5′-CCGGCCAAGATTTGTACTCTGATAACTCGAGTTATCAGAGTA-CAAATCTTGGTTTTTG-3′, *Orp8.2* shRNA loop sequence 5′-CCGGAGATCGA-AAGACAGCACTTTACTCGAGTAAAGTGCTGTCTTTCGATCTTTTTTG-3′) (Sigma-Aldrich) according to the manufacturer's instructions. Transduced cells were selected with 2.5 µg ml^{-1} puromycin. Puromycin-resistant clones were expanded and assayed for ORP8 expression by western-blot analysis. The effect of ORP8 knockdown on insulin-stimulated AKT phopshorylation was examined in overnight-serum-depleted cells. After stimulation with human insulin (Sigma-Aldrich) for 20 min at 37 °C, the medium was removed and the cells were immediately lysed with ice-cold lysis buffer (25 mM Tris-HCl at pH 8.0, 10 mM MgCl$_2$, 100 mM NaCl, 1% Triton X-100, 10% glycerol, 1× protease inhibitor cocktail (Roche complete tablets) and 1 mM dithiothreitol).

Dual luciferase reporter assay. For reporter construct generation either wild-type or mutated miR-143 binding sites in the 3′ UTR of ORP8 were inserted downstream of the firefly-luciferase open reading frame. Hepa1–6 cells were plated on 24-well plates and transfected with 500 ng DNA using Lipofectamine 2000 transfection reagent (Invitrogen). Dual luciferase reporter assays were carried out 48 h after transfection using a Luciferase Assay System (Promega) according to the manufacturer's instructions.

Statistical methods. Data sets were analysed for statistical significance using a two-tailed unpaired Student t-test. All values shown are means ± s.e.m. *$P \leq$ 0.05,**$P \leq 0.01$, ***$P \leq 0.001$ versus control.

53. Pfeffer, S., Lagos-Quintana, M. & Tuschl, T. *Current Protocols in Molecular Biology* Vol. 24 (2005).
54. Konner, A. C. *et al.* Insulin action in AgRP-expressing neurons is required for suppression of hepatic glucose production. *Cell Metab.* **5,** 438–449 (2007).
55. Plum, L. *et al.* Enhanced leptin-stimulated Pi3k activation in the CNS promotes white adipose tissue transdifferentiation. *Cell Metab.* **6,** 431–445 (2007).
56. Mauer, J. *et al.* Myeloid cell-restricted insulin receptor deficiency protects against obesity-induced inflammation and systemic insulin resistance. *PLoS Genet.* **6,** e1000938 (2010).
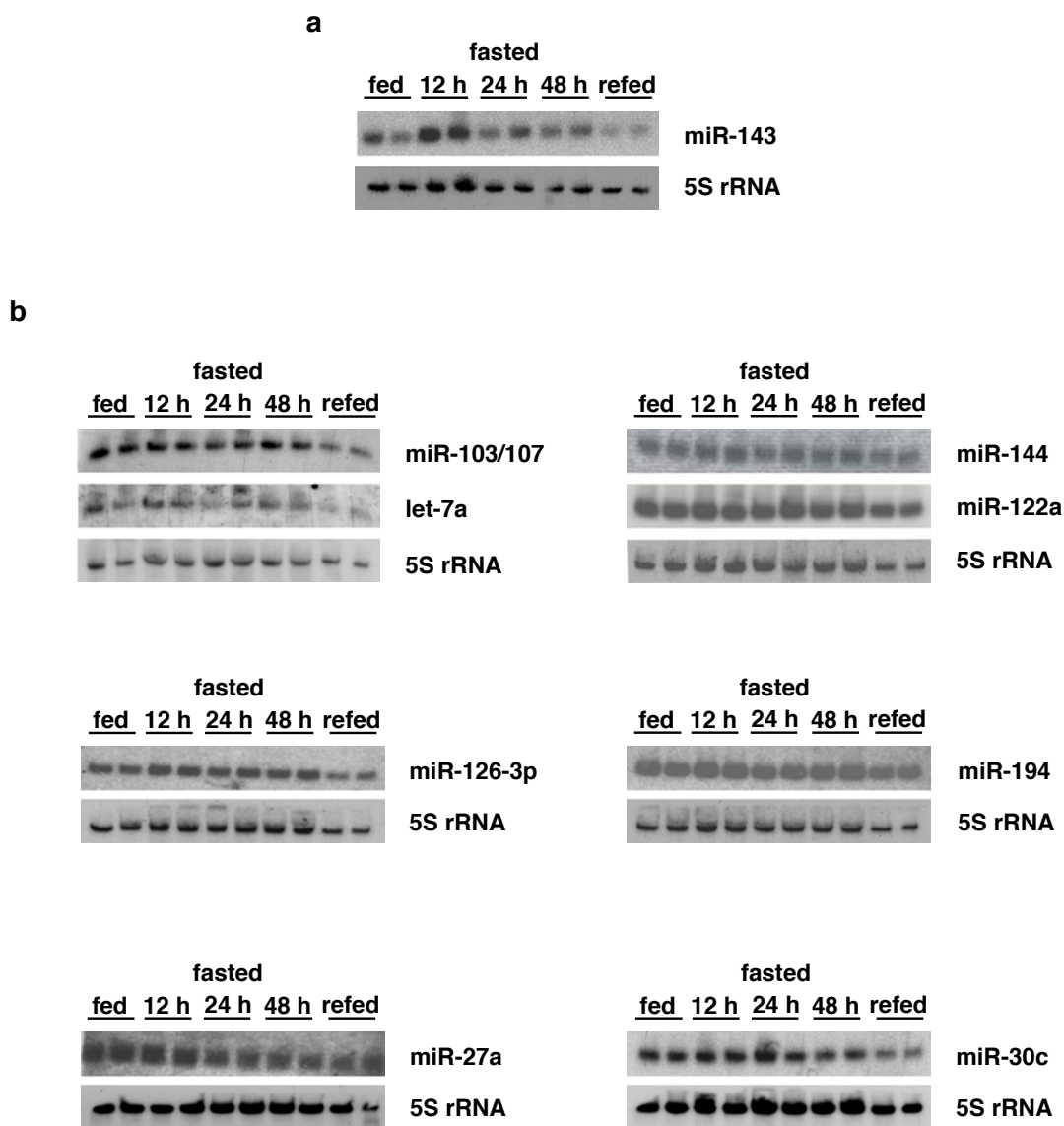
Figure S1 Northern blot analysis of miR-143 expression dependent on feeding conditions. **a** Northern blot analysis of miR-143 expression in liver of random fed, 12-48 hours fasted and refed mice. 5S rRNA was used as loading control. **b** Representative Northern blot analyses of miRNA expression in liver of random fed, 12-48 hours fasted and refed animals using the indicated miRNA probes. 5S rRNA was used as loading control. In total, livers of three mice per condition were analyzed for feeding status-dependent regulation of miRNA expression.
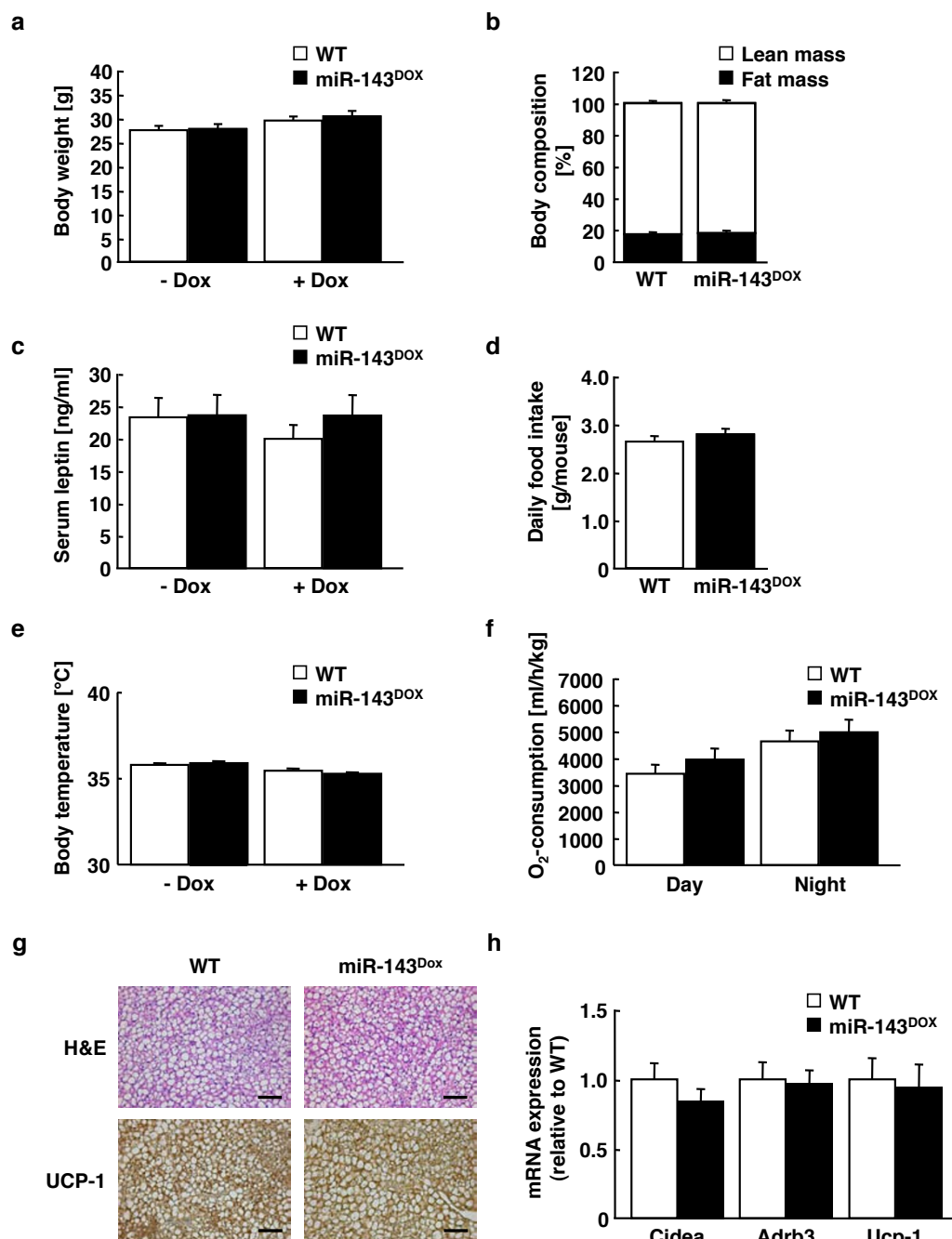
Figure S2 Unaltered energy homeostasis in miR-143-overexpressing mice. **a** Body weight of miR-143^{DOX} mice (filled bars; n≥24) and WT littermate controls (open bars; n≥24) before and after doxycycline administration. **b** Body composition of miR-143^{DOX} mice (n=10) and WT littermate controls (n=11) measured by nuclear magnetic resonance (filled bars = fat mass; open bars = lean mass). **c** Serum leptin levels of miR-143^{DOX} mice (filled bars; - Dox n=23, + Dox n=18) and WT littermate controls (open bars; - Dox n=24, + Dox n=21) before and after administration. Concentrations were measured in random fed mice. **d** Daily food intake of miR-143^{DOX} mice (filled bars; n=7) and WT littermate controls (open bars; n=6) during doxycycline administration. **e** Body temperature of miR-143^{DOX} mice (filled bars; n=7) and WT littermate controls (open bars; n=11) before and doxycycline administration. **f** Oxygen (O_2) consumption of miR-143^{DOX} mice (filled bars; n=7) and WT littermate controls (open bars; n=9). Presented data are average values obtained during indirect calorimetry measurements of at least 48 hours. **g** Hematoxylin and eosin (H&E) and UCP-1 staining of brown adipose tissue in miR-143^{DOX} mice and WT littermate controls. Scale bars 50 µm. **h** Real-time PCR analysis of Cidea, Adrb3 and Ucp-1 mRNA expression in brown adipose tissue of miR-143^{DOX} mice (filled bars; n = 12) and WT littermate controls (open bars; n = 18). Expression of mRNAs was normalized to Gusb and Hprt mRNA and set to 1 in WT controls. All error bars indicate s.e.m.
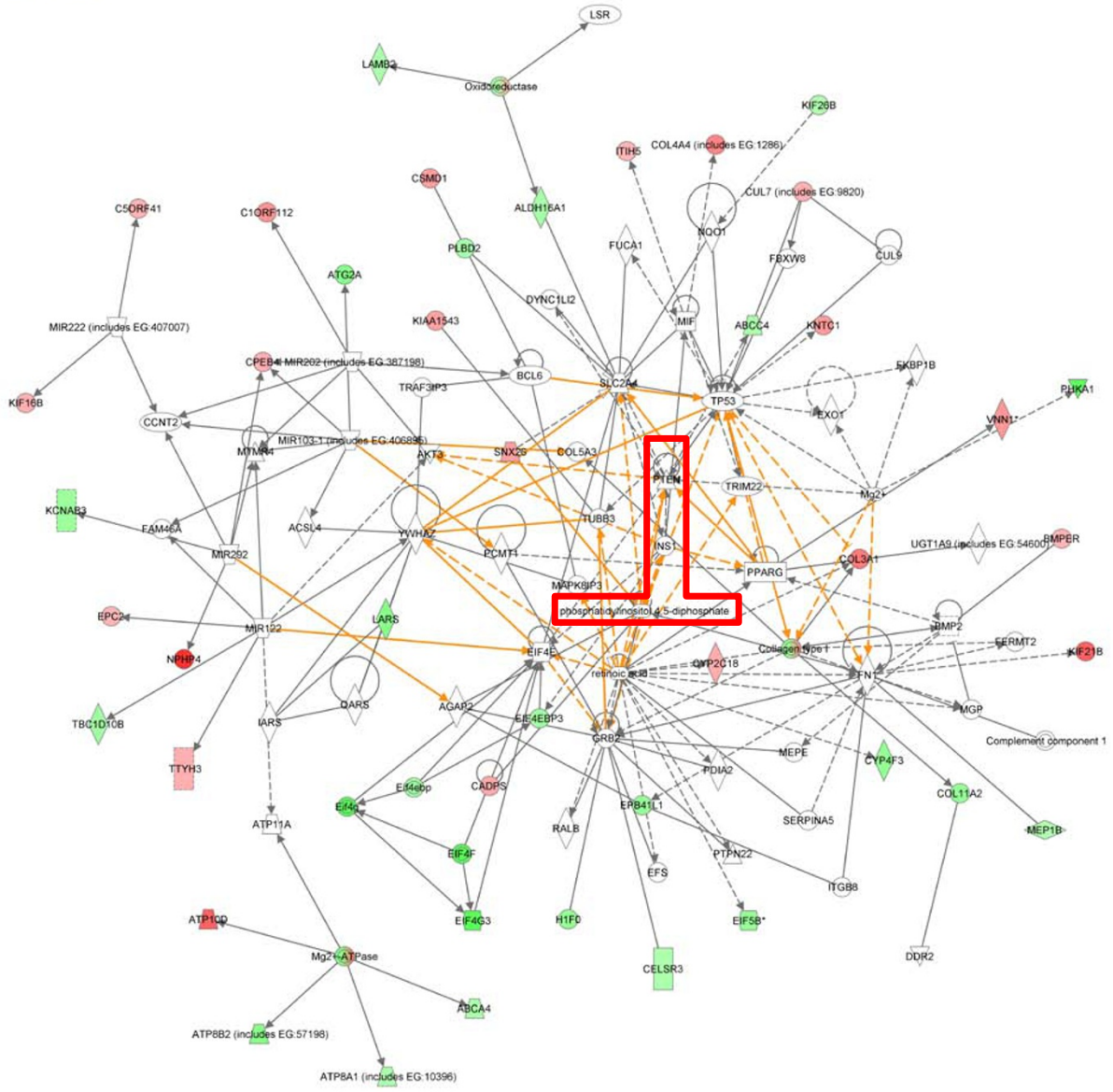
Figure S3 Network analysis of genes with altered expression in miR-143 overexpressing mice reveals overlap at insulin-dependent PI3k signaling. Schematic representation of network analysis using Ingenuity Pathway Analysis Software. Labeling of genes according to Ingenuity Systems.
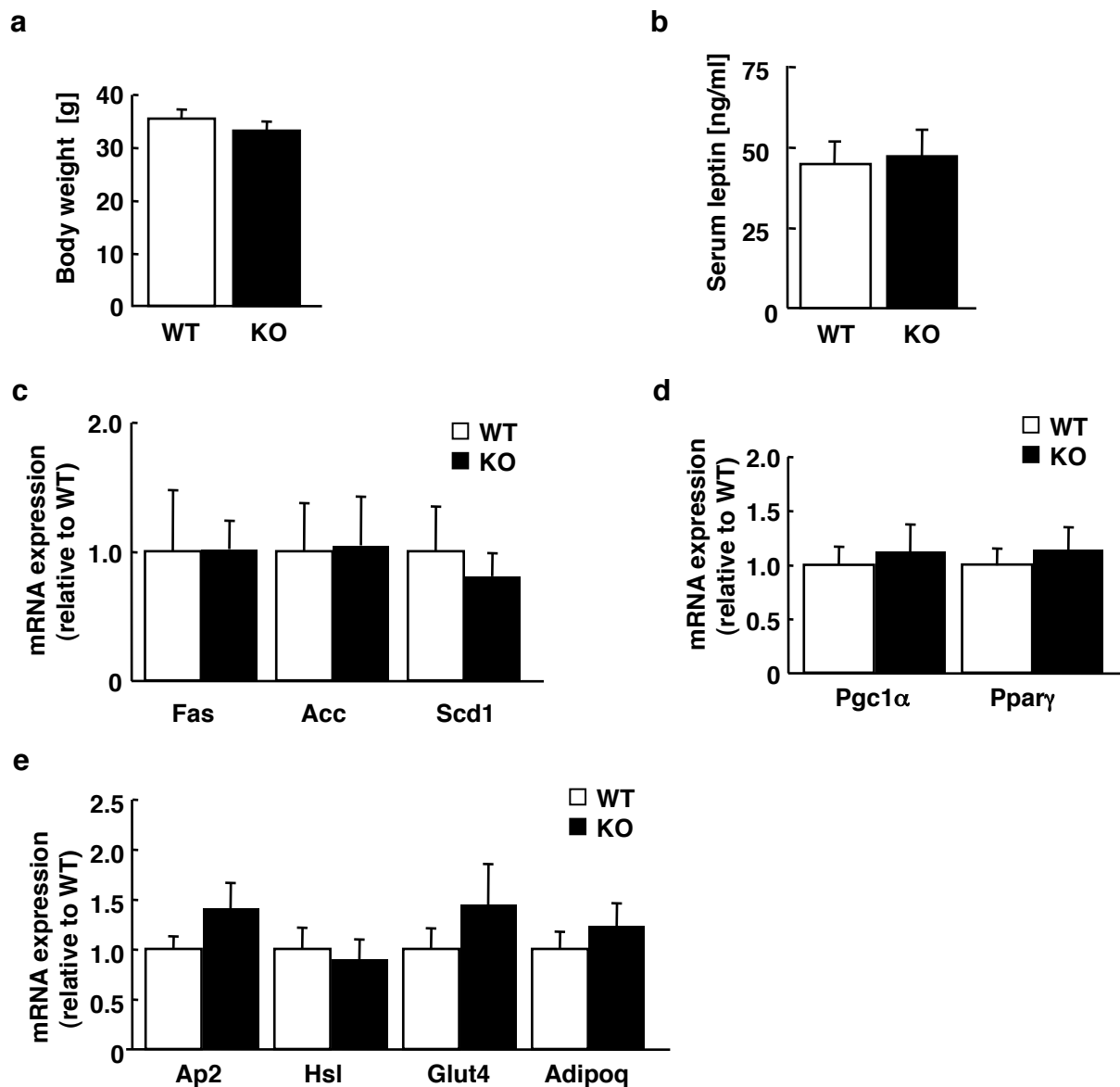
Figure S4 Unaltered body weight, serum leptin levels and white adipose tissue gene expression in miR-143-145 deficient mice. **a** Body weight of miR-143-145 KO mice (filled bars; n=12) and WT littermate controls (open bars; n=13) on high fat diet. **b** Serum leptin levels of miR-143-145 KO mice (filled bars; n=8) and WT littermate controls (open bars; n=9) on high fat diet. Concentrations were measured in random fed mice. **c** Real-time PCR analysis of Ap2, Hsl, Glut4 and Adipoq mRNA expression in white adipose tissue of miR-143-145 KO mice (filled bars; n=5) and WT littermate controls (open bars; n=5) on high fat diet. **d** Real-time PCR analysis of Pgc1α and Pparγ mRNA expression in white adipose tissue of miR-143-145 KO mice (filled bars; n=5) and WT littermate controls (open bars; n=5) on high fat diet. **e** Real-time PCR analysis Fas, Acc and Scd-1 mRNA expression in white adipose tissue miR-143-145 KO mice (filled bars; n=5) and WT littermate controls (open bars; n=5) on high fat diet. All error bars indicate s.e.m. For real-time analyses expression of mRNAs was normalized to Gusb and Hprt mRNA and set to 1 in WT controls.

Figure 1a
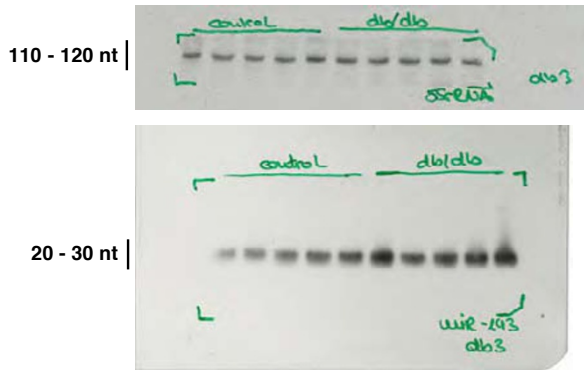
Figure 1b
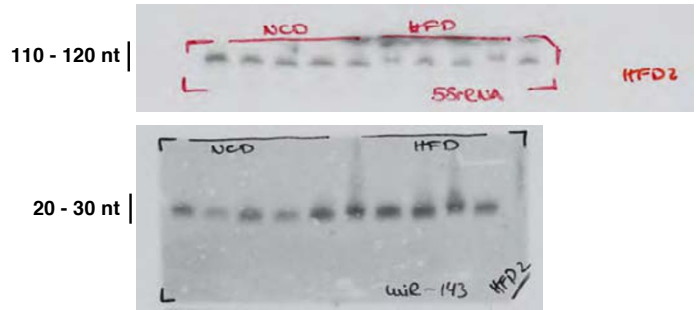
Figure 2d
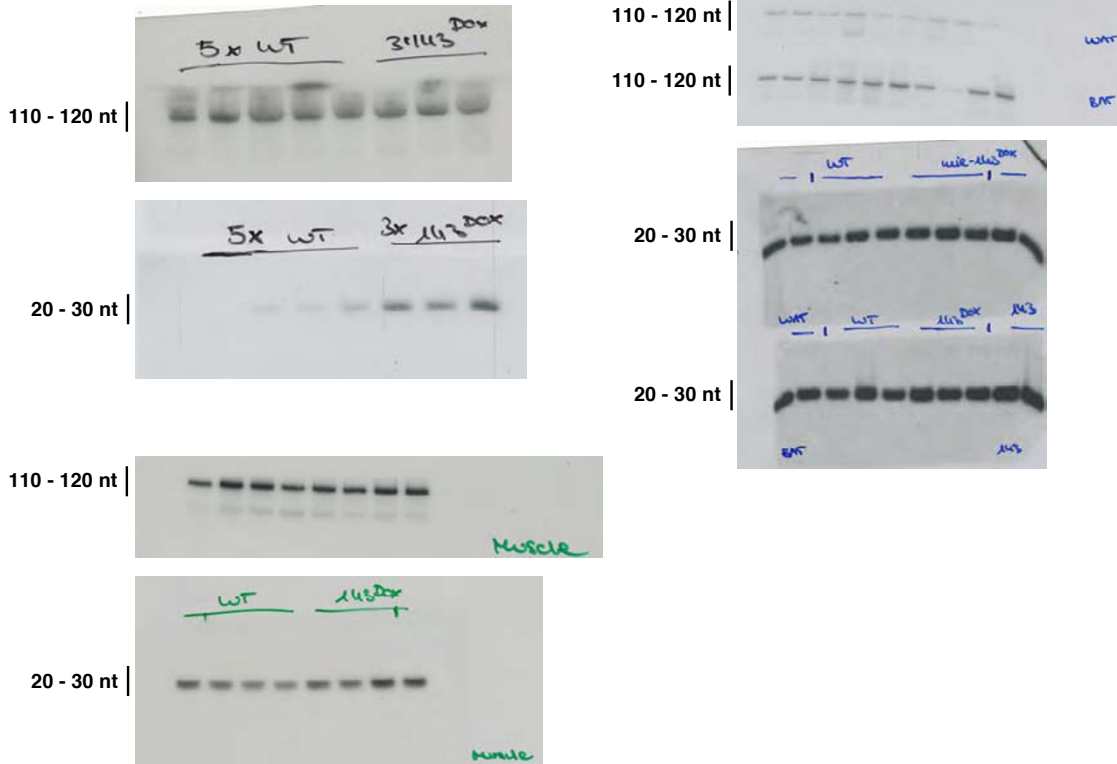
Figure S5 Full scans

Figure 2f
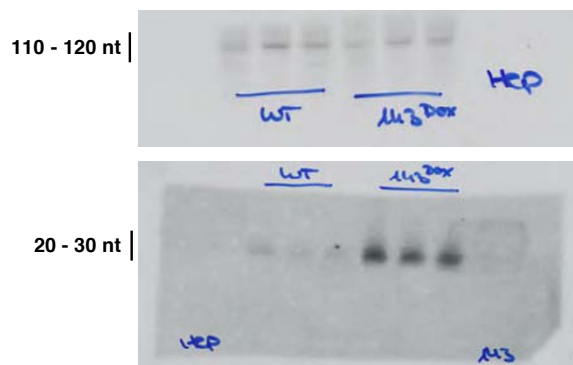
Figure 2g
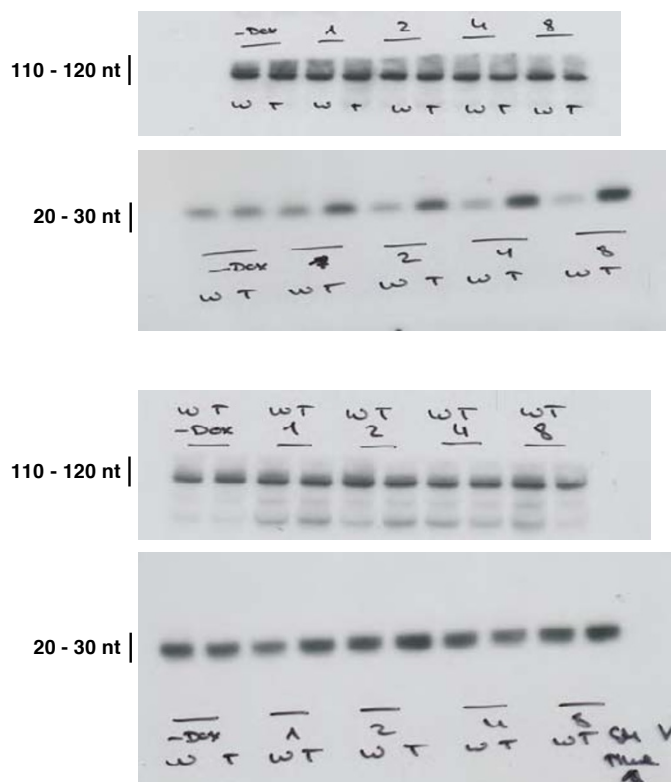
Figure S5 continued

Figure 5a
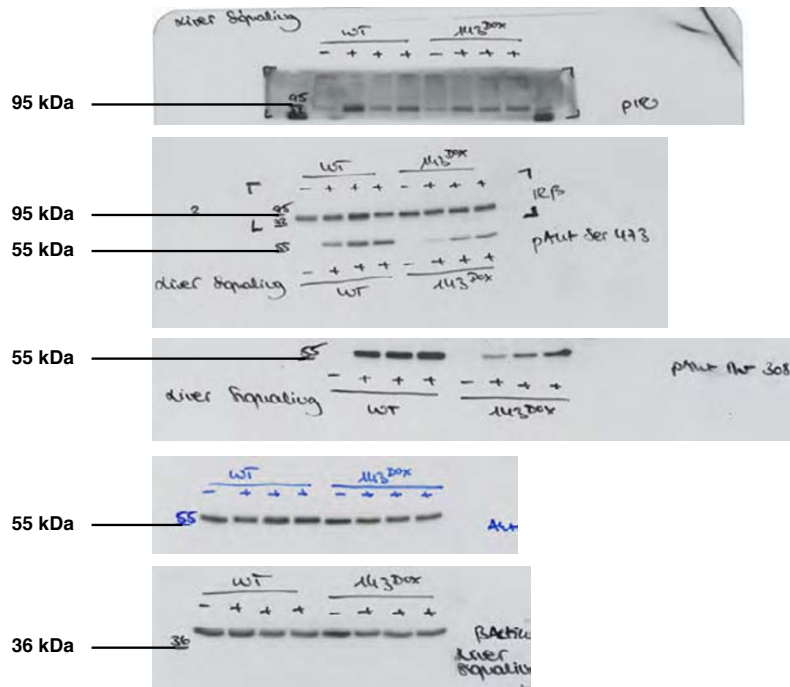
Figure 5b
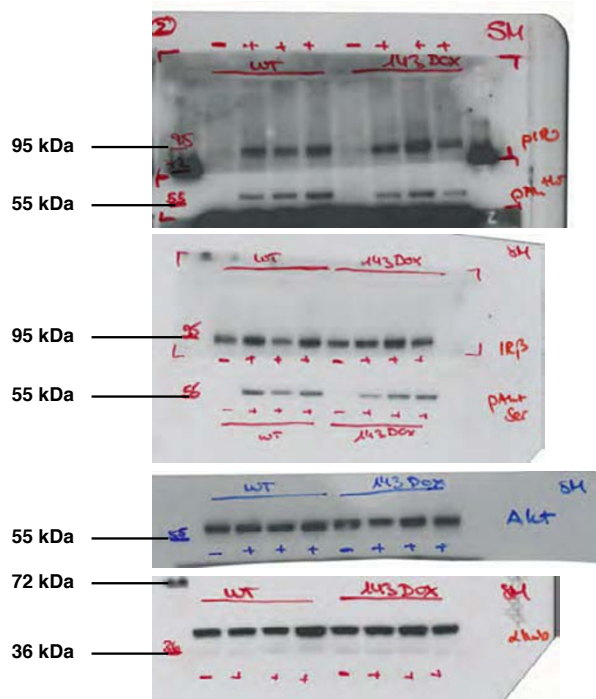
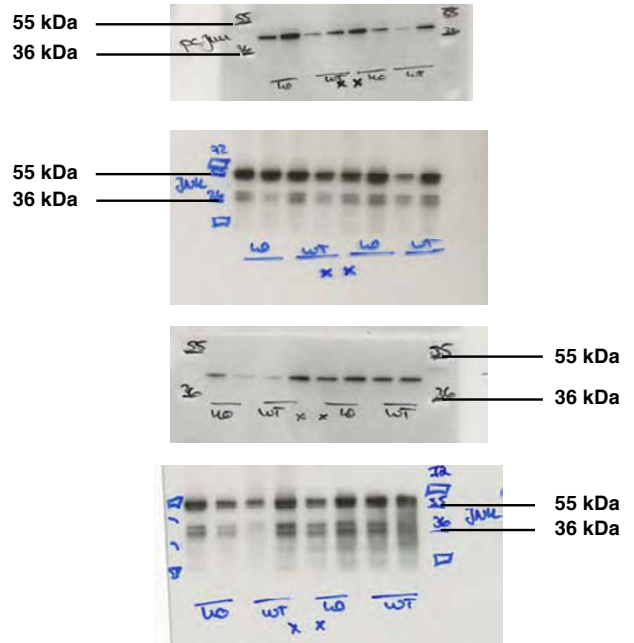**Figure S5 continued**

Figure 6c
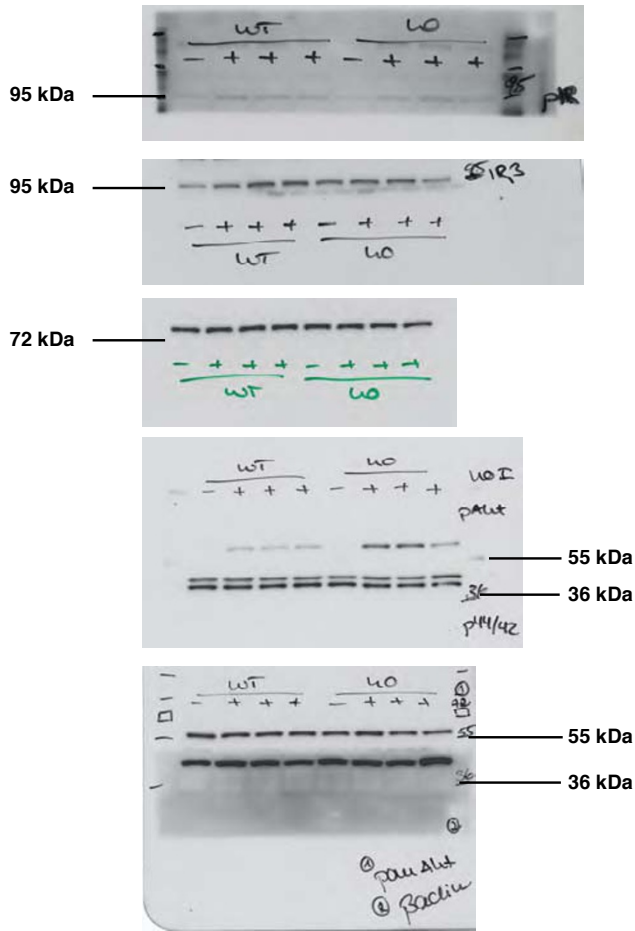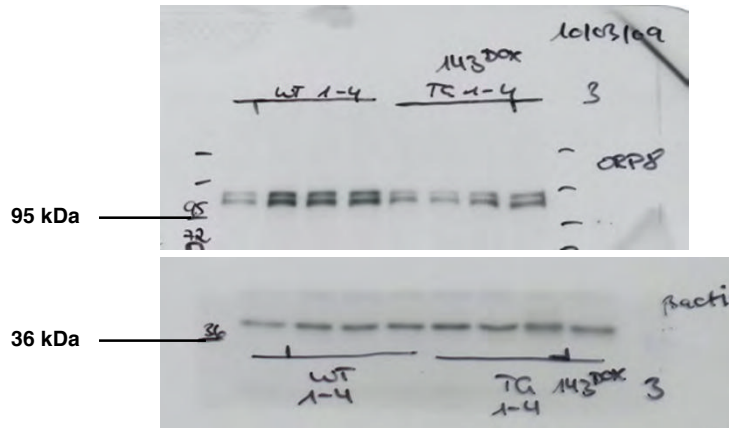

Figure 6g

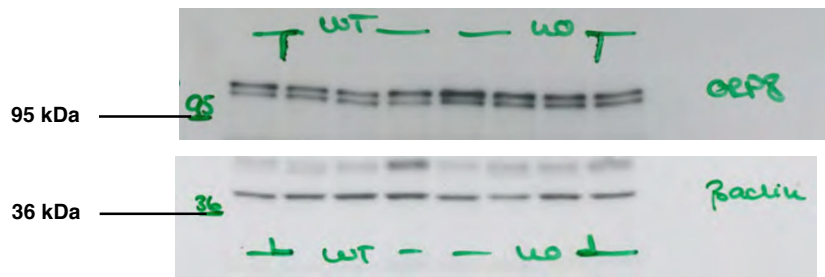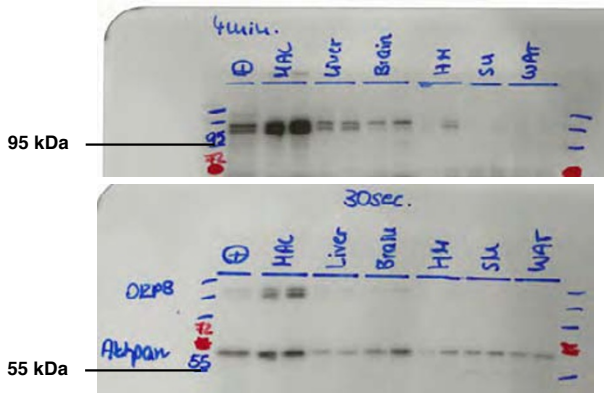**Figure S5 continued**

Figure 7c

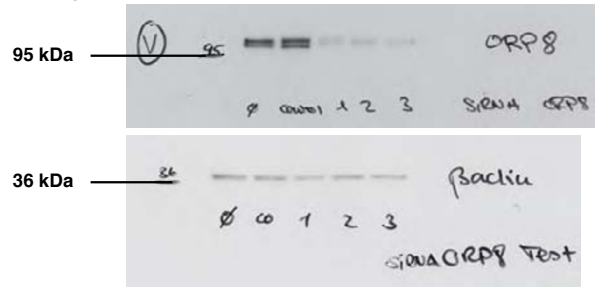Figure 7e

Figure S5 continued
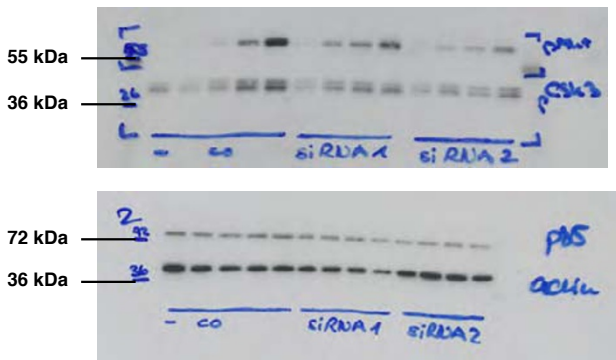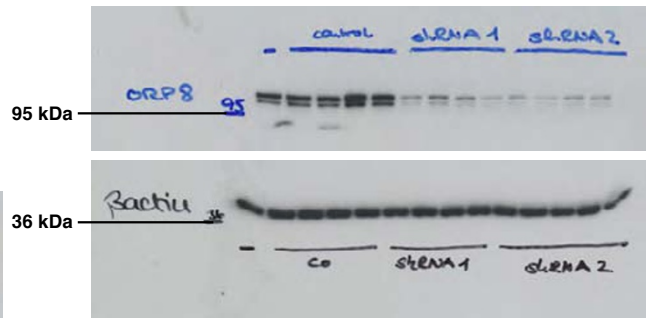
Figure 8a

Figure 8b

Figure 8c
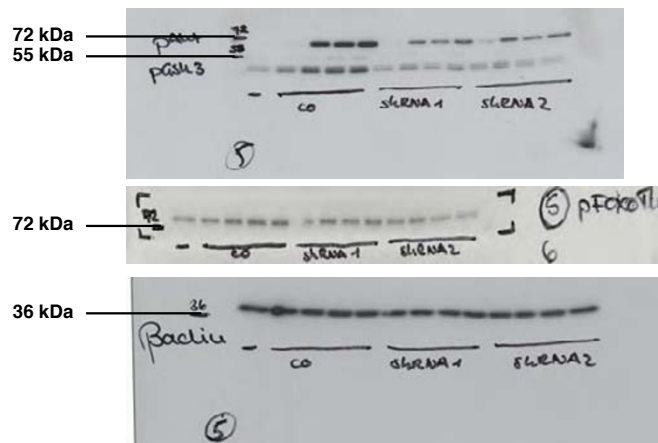

Figure 8d

Figure 8e

Figure S5 continued

Supplementary table legends

Table S1a Bioinformatic analyses of cloned small RNAs
Table S1b Summary of cloned and verified hepatic miRNAs
Table S2 Gene expression analyses of miR-143 overexpressing mice (.xls file)
Table S3 *In vivo* SILAC analyses of miR-143 overexpressing mice (.xls file)
Table S4 Potential hepatic miR-143 targets identified by *in vivo* SILAC